MEDDELANDEN
FRÅN
STATENS SKEPPSPROVNINGSANSTALT
(PUBLICATIONS OF THE SWEDISH STATE SHIPBUILDING EXPERIMENTAL TANK)
Nr 48 GÖTEBORG 1961

# CAVITATION TUNNEL TESTS WITH MERCHANT SHIP PROPELLERS

BY

HANS LINDGREN

Read before
The Institution of Engineers and Shipbuilders in Scotland
April 1961


AKADEMIFÖRLAGET / GUMPERTS, GÖTEBORG
GYLDENDALSKE BOGHANDEL / NORDISK FORLAG, KØBENHAVN
AKATEEMINEN KIRJAKAUPPA / AKADEMISKA BOKHANDELN, HELSINGFORS
WILLIAM HEINEMANN LTD, LONDON, MELBOURNE, TORONTO

SCANDINAVIAN UNIVERSITY BOOKS

*Gyldendalske Boghandel / Nordisk Forlag, København*
*Svenska Bokförlaget / P. A. Norstedt & Söner — Albert Bonnier, Stockholm*
*Akademiförlaget / Gumperts, Göteborg*
*Akateeminen Kirjakauppa / Akademiska Bokhandeln, Helsingfors*
*William Heinemann Ltd, London, Melbourne, Toronto*

GÖTEBORG 1961
ELANDERS BOKTRYCKERI AKTIEBOLAG

## 1. Introduction

Increased loading on modern cargo ship propellers, necessitated by the greater speed and size of the ships, has greatly increased the risk of damage due to cavitation erosion. Whilst blade area ratios of 40—50% were considered to be sufficient 15 years ago, values of up to 70% are not unusual nowadays.

As is well known, the propeller of a single screw ship works in a very unfavourable velocity distribution. It is therefore not astonishing to note that cavitation tunnel authorities all over the world regard the problem of reproducing the non-uniform flow conditions in which a ship propeller operates as a highly important topic (*vide* Decisions and Recommendations of the 9th International Towing Tank Conference (ITTC) in Paris 1960).

At the Swedish State Shipbuilding Experimental Tank (SSPA) in Gothenburg, a great deal of work during recent years has been devoted to studying the possibilities of reproducing ship wake distributions in the cavitation tunnel. Some notes on this work will be presented. Furthermore, the results of some systematic tests carried out to explore the influence of the irregular flow on the extent of propeller cavitation and the importance of blade area ratio and profile shape will be given. Finally the scale effects will be dealt with, together with some results from comparisons between model cavitation pictures and full scale propeller erosion patterns.

## 2. The Wake Distribution

The wake distribution, to be reproduced in the cavitation tunnel, can be measured on a ship model in an open towing tank with the help of pitot tubes. Fig. 1 gives the iso-wake curves for a fine cargo ship ($\delta_{pp}=0.675$). The circumferential variations at one radius, when a blade passes the top position are shown to the right in Fig. 1. A

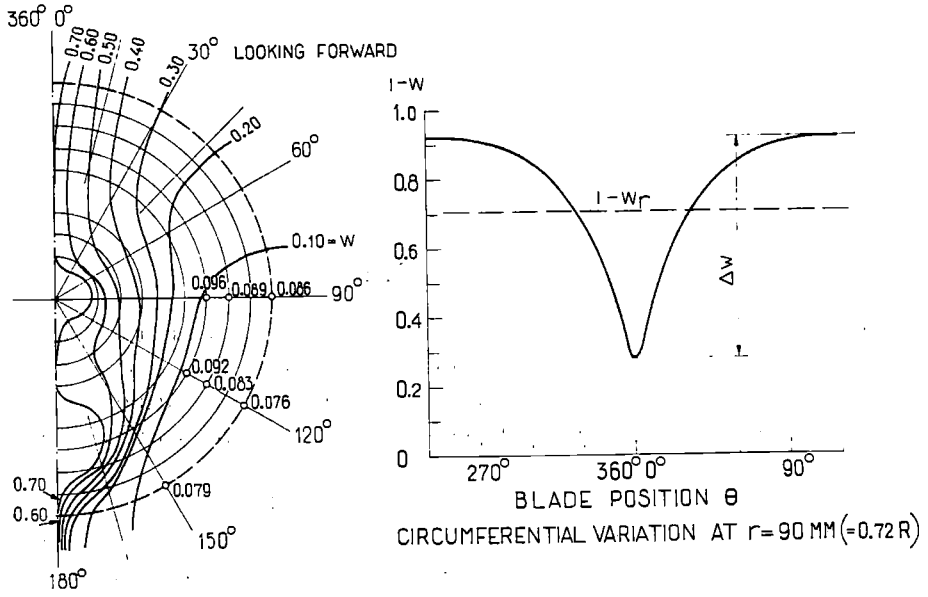


Fig. 1. Model No. 720, Wake Distribution.

number of wake distributions for different single and twin screw cargo vessels have been analyzed in Figs. 2—4, primarily to show the influence of fullness and shape of the afterbody sections on the peripheral and radial velocity variations. The nominal mean wake factor is defined as

$$w_N = \frac{\int_{r_0}^{R} w_r r dr}{1/2\,(R^2 - r_0^2)},$$

where $$w_r = \frac{\int_0^{2\pi} w d\theta}{2\pi}$$

$w$=local wake fraction

$R$=propeller radius, $r_0$=boss radius

With regard to the radial variation of the circumferential mean wake $w_r$, it can be concluded that for single screw ships the section shape is of primary importance, Fig. 3. The three models compared

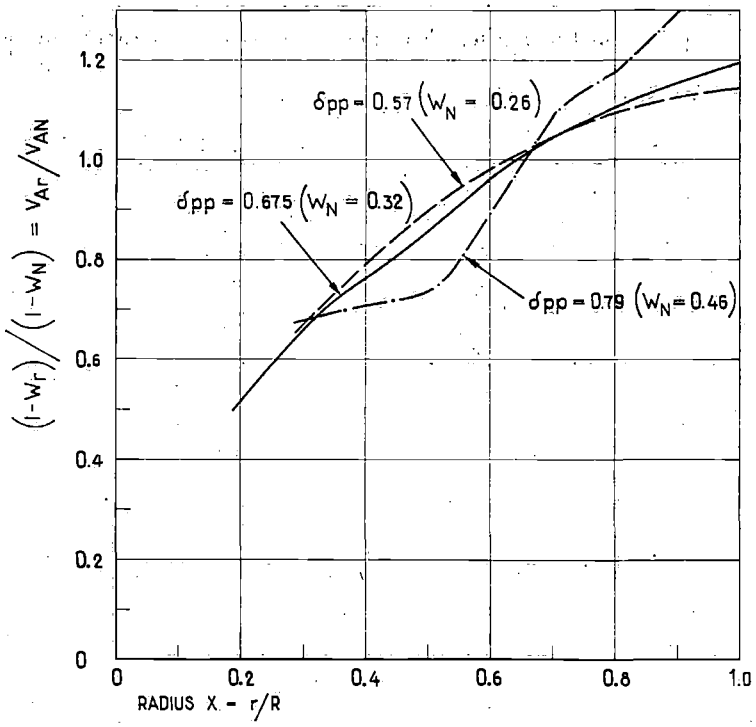


Fig. 2. Influence of Block Coefficient on the Radial Wake Distribution.

here belong to a model family with block coefficients, $\delta_{pp}=0.675$ which was the subject of experiments described more fully in [1][1]). Furthermore, as could be expected, the curves for the twin screw ships are less steep. In Fig. 2, single screw models with approximately moderate U-shaped afterbody sections are compared. The curves representing $\delta_{pp}=0.57$ and 0.675 are very similar, but for the fuller ship, the slope of the curve increases considerably.

The circumferential variations are represented by the factors $\Delta w/(1-w_r)$ in Fig. 4 ($\Delta w$ and $w_r$ are defined above and in Fig. 1). The variations increase with the block coefficient and are very small for the destroyer, but larger for the twin-screw tanker than for the single- screw ships. The influence of the shape of the afterbody sections is fairly small.

As is well known, the advance coefficient $J=\frac{V_A}{DN}$ is of primary

[1]) The figures within brackets refer to the references in Section 9.

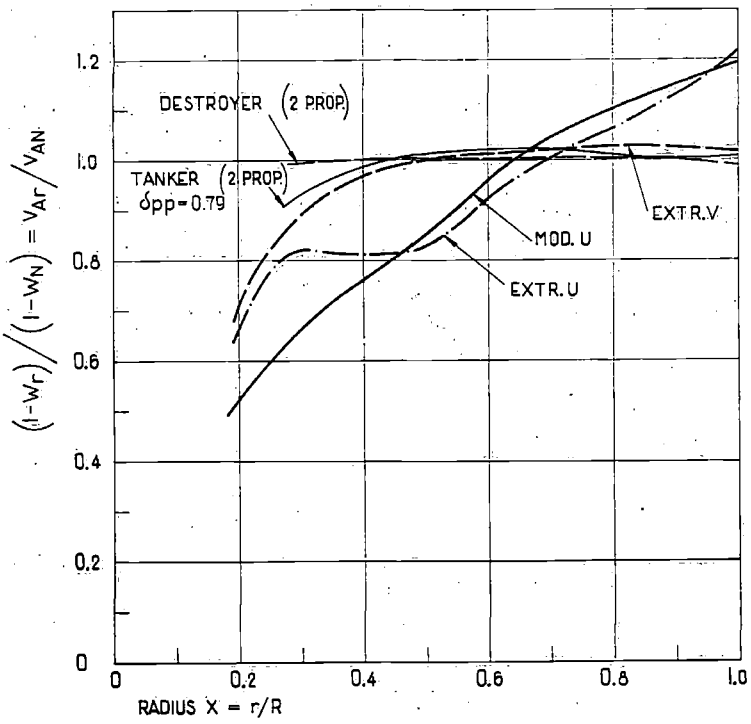


Fig. 3. Influence of Section Shape on the Radial Wake Distribution.

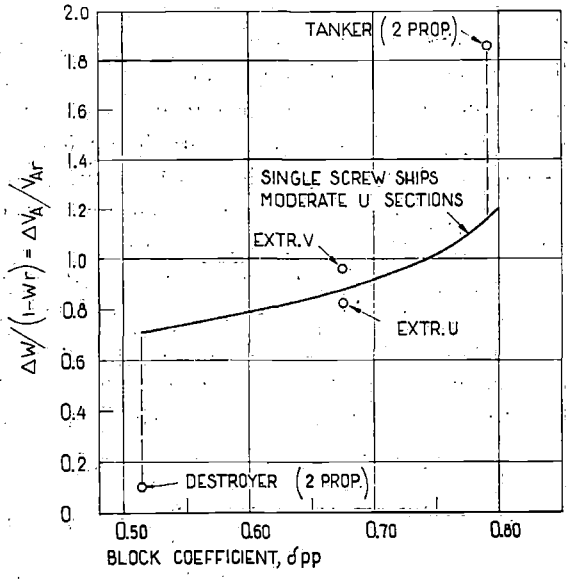


Fig. 4. Circumferential Wake Variations at 0.75 *R*.

importance to the cavitation characteristics of a propeller. Determination of the effective wake fraction is therefore essential. Experience and theory have shown that the wake scale effects can not be neglected, whilst the scale effects on the other propulsive components seem to be of less importance [2]. At SSPA the wake scale effects are normally treated according to the following method: —

Statistics obtained by analyzing ship trial results and comparing them with model test results, give information on the correlation factors $A$ and $B$ (see also Ref. [3]), where

$$A = \frac{P_{PS}}{P_{PM}}$$

$$B = \frac{N_S}{N_M}$$

$P_P$=propeller shaft power

$N$=number of revolutions

Suffix $S$ and $M$ refer to ship and model respectively.

For an actual ship $P_{PS}$ and $N_S$ and thus $K_{QS} = \frac{Q_S}{\varrho D^5 N_S^2}$ can be calculated from the model test results, using the correlation factors above. The corresponding $J$-value can be read from the open-water diagram assuming no scale effect on the $K_Q$-$J$-curve.

The ship wake, $w_S$, then is obtained as

$$w_S = 1 - \frac{JD_S N_S}{V_S}$$

The $w_S$-values so obtained are normally between 0.05 and 0.10 lower than the corresponding model wake values. However, due to increasing bottom roughness, the wake increases with time and it is not unusual that the value one or two months after docking is similar to or higher than the model wake. Therefore, at SSPA cavitation tests are normally carried out at a load condition corresponding to the model wake as well as the wake predicted for the ship with clean bottom.

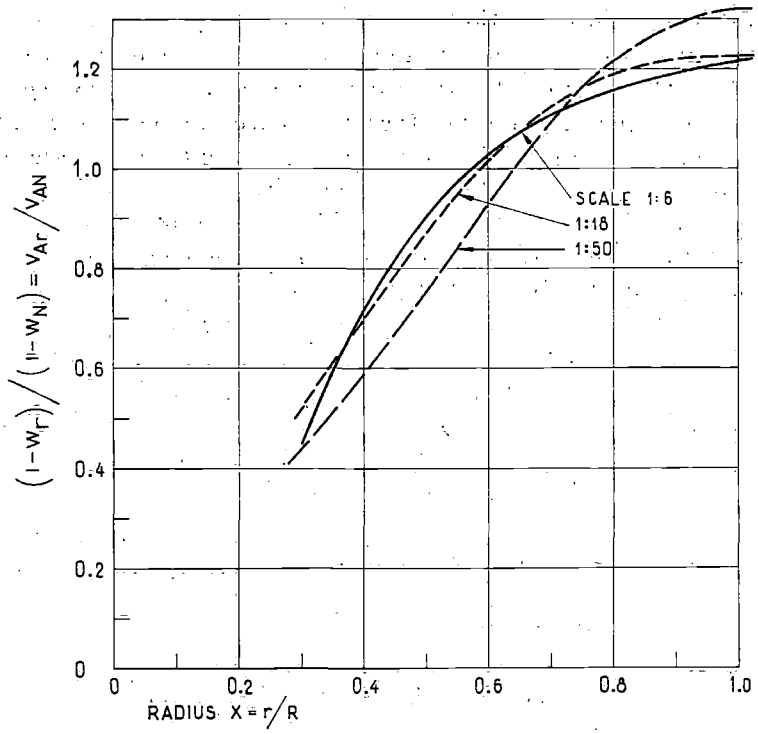


Fig. 5. NSMB Victory Series. Radial Wake Distributions.

The reason why the ship trial wake is lower than the model wake is that the ship boundary layer, due to higher REYNOLDS number, is relatively thinner than the boundary layer of the model. It can therefore be expected that the scale effect influences not only the effective wake, as assumed with the above method, but also the wake distribution. However, too little is known about the ship wake distributions at present to correct for this in the model tests. Some information can be gained by analyzing the results of the Dutch VICTORY test series [4]. In Fig. 5 the radial wake distributions for three geometrically similar models with scale 1: 50, 1: 18 and 1: 6 are compared. As could be expected the curves become steeper with diminishing model size due to increasing boundary layer thickness. Concerning the most interesting radii near the tip, no clear influence by the scale on the circumferential wake variation could be concluded.

## 3. Irregular Flow Distribution in Cavitation Tunnels

Several possible methods of studying propeller cavitation in non-uniform flow conditions in a cavitation tunnel have been proposed. The simplest method is to calculate the local $J$ and $\sigma$-values at different angular blade positions and reproduce these conditions spot after spot in homogeneous flow. This eliminates all the influences of differences due to interference between the blades and between different propeller radii as well as those due to irregularity of the flow. This method will be discussed further in Section 4.

The next alternative is to try to reproduce in the tunnel the wake distribution measured in the towing tank. Astonishingly few institutions have reported results from this type of work, but it appears that extensive work is going on at the present time.

Different methods of producing irregular flow in cavitation tunnels have been proposed, and a summary was presented by VAN MANEN at the 9th ITTC in Paris, 1960 [5]. Generally three different methods are in use namely: —

*A*. A more or less complete ship model installed in the cavitation tunnel in front of the propeller model

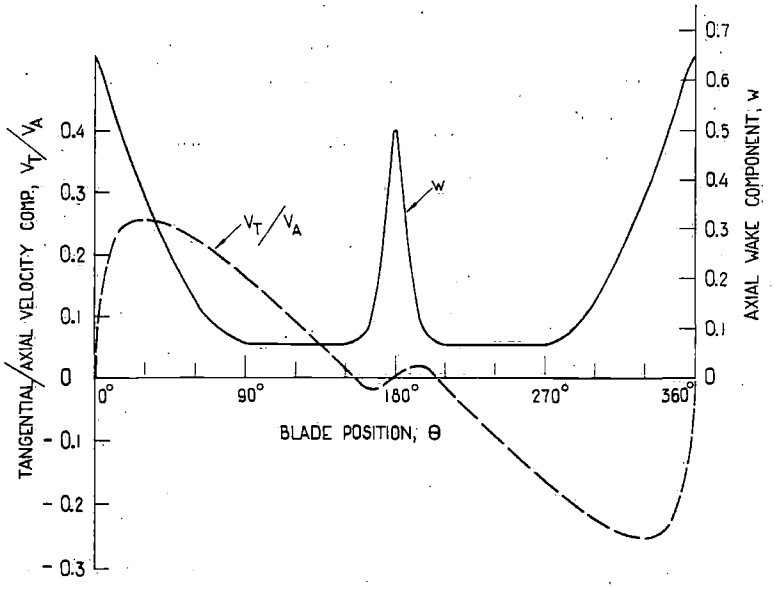


Fig. 6. Relation Between Tangential and Axial Velocity Components.

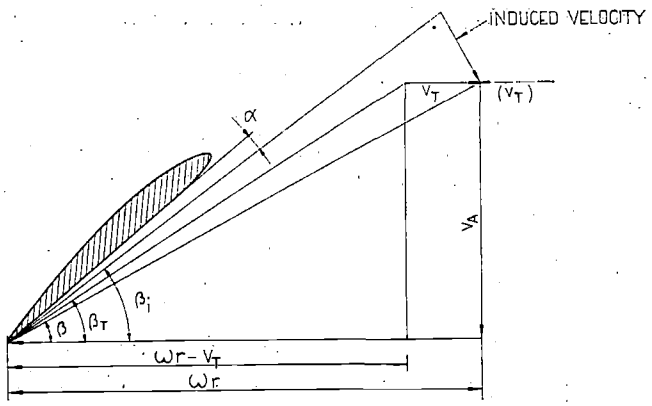


Fig. 7. Velocity Diagram.

*B.* Wake-producing transverse wire meshes in front of the propeller model

*C.* Flow regulator of the type developed by the NSMB — Wageningen

With the methods *B* and *C* it is possible to get very good agreement between the axial wake distributions measured in the towing tank and in the cavitation tunnel. On the other hand the flow directions, and especially the tangential flow components are ignored. Fig. 6 shows the relationship between the tangential and axial velocities, together with the axial wake factor, for a fast cargo ship, studied by TACHMINDJI and LEWIS [6]. The curves correspond to a radius of about 0.75 *R*.

From the velocity diagram, Fig. 7, it appears that due to the tangential velocities, $V_T$, the hydrodynamic pitch angle, $\beta$, changes from

$$tg\beta = \frac{V_A}{x\omega R}\left(= \frac{\lambda}{x}\right)$$

to

$$tg\beta_T = \frac{V_A}{x\omega R - V_T} = \frac{\lambda}{x - \lambda\dfrac{V_T}{V_A}}$$

where $\lambda = \dfrac{V_A}{\pi N D}$ and $x = r/R$

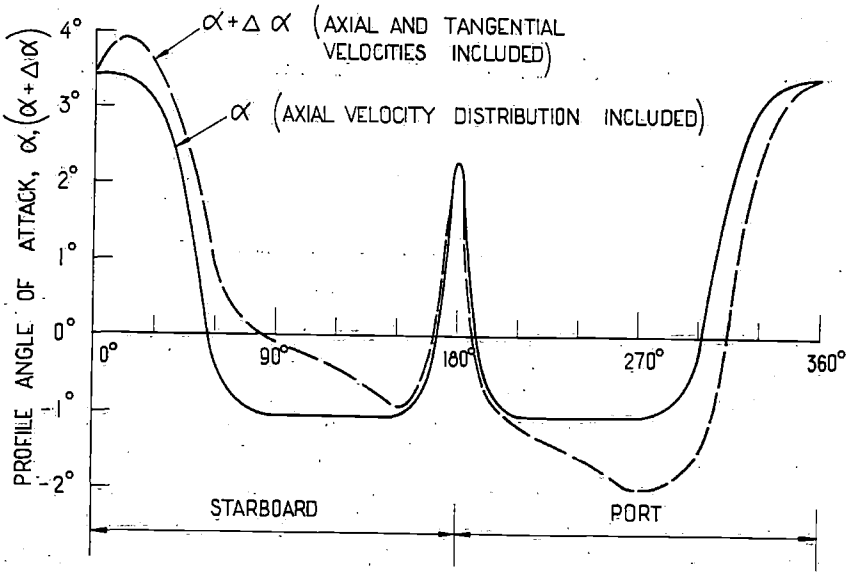


Fig. 8. Variation of the Profile Angle of Attack at 0.75 $R$.

A first approximation of the influence of the tangential velocities on the profile angle of attack is

$$\Delta\alpha=\beta_T-\beta$$

For propeller No. P 755 (see Section 4) the relationship between $\alpha$ and $J=\frac{V_A}{DN}$ at $r=0.75\ R$, has been obtained using the equivalent profile method as presented by LERBS [7]. This relationship has been used to obtain the circumferential variation of $\alpha$, due to the axial wake variation, Fig. 8. Furthermore $(\alpha+\Delta\alpha)$ is given, whereby the $\Delta\alpha$-values are obtained according to the above equation. The propeller is assumed to operate in the wake distribution shown in Fig. 6, and at a loading corresponding to shock-free entrance ($\alpha=0$) at the mean wake. The calculations on which Fig. 8 are based are very schematic. For instance, the difference in the blade interference in homogeneous and non-homogeneous flow has been disregarded. Furthermore the flow has been assumed to be constant in each spot. However, the figure can be used for trend studies, and it can be concluded that the profile angle of attack varies between about $+4$ and $-2$ degrees. Due

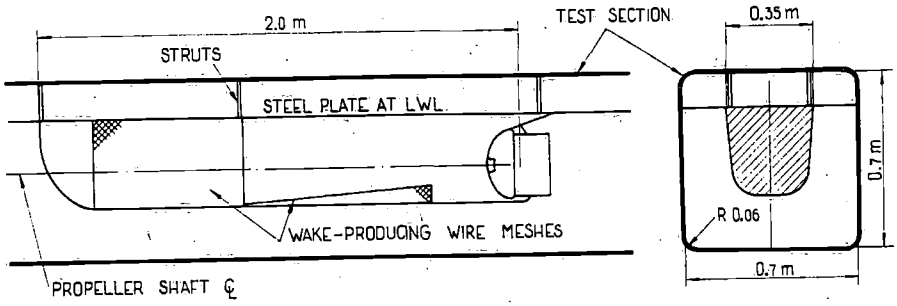


Fig. 9. Installation of a Dummy Model in the Test Section.

to the influence of the tangential components, the maximum angle occurs on the starboard side of the stern (right—handed propeller) and the greatest negative angle occurs on the port side at about 270°. Frequent tests with propellers abaft afterbody dummies have confirmed this by the appearance of extensive suction and pressure side cavitation in the corresponding blade positions. The negative angle of attack at the 270° position is nearly doubled due to the tangential velocity component.

Primarily to get the influences from all the velocity components, it was decided at SSPA to try to use as complete afterbody dummies as possible in the cavitation tunnel to simulate the velocity field. Tests have been carried out with models of different type and size and some experience has been gained partly of negative nature.

A complete ship model in a cavitation tunnel can be used only if the cavitation tunnel is very large or if the ship model is very small. The SSPA cavitation tunnel [8] has a test section which is 2.4 m (7.9 ft.) in length and has an area of 0.7 m (27.5 in.) square. A normal ship model is about 6.5 m (21 ft.) in length and 0.9 m (3 ft.) in breadth. A breadth of 0.45 m (17.7 in.) on the dummy was regarded to be the upper limit that could be used. Experience has also shown that this breadth is too large especially for fuller ships, as heavy separation of the flow is created. Fig. 9 shows in principle the installation of an afterbody dummy in the cavitation tunnel. The dummy is fixed to a horizontal plate corresponding to the load waterline. The length of the struts is chosen so that the normal propeller shaft in the centre of the test section can be used.

In Fig. 10 some waterlines of model No. 720 are given, together with the corresponding waterlines of dummies Nos. 922 and 950,

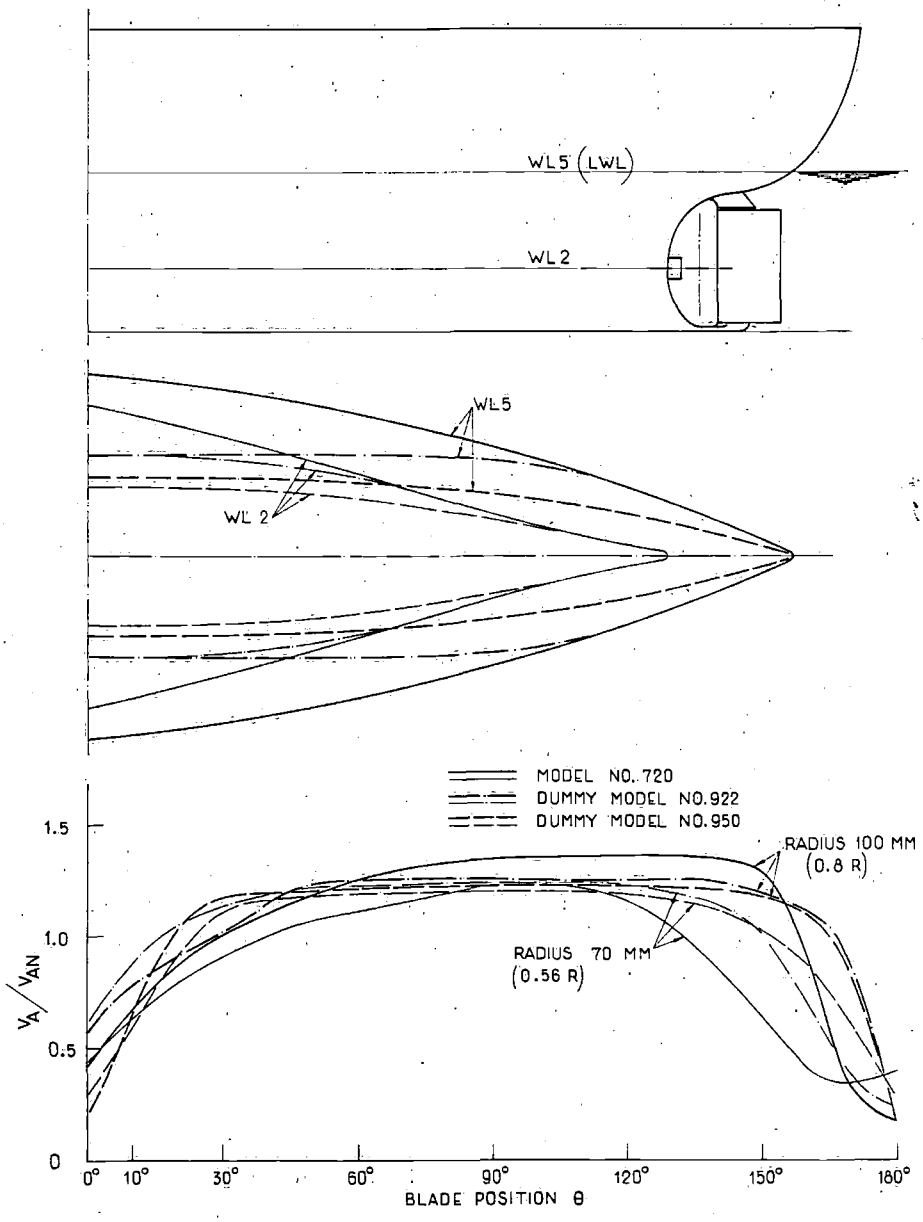


**Fig. 10. Comparisons Between Ship Model No. 720 and Dummy Models Nos. 922 and 950.**

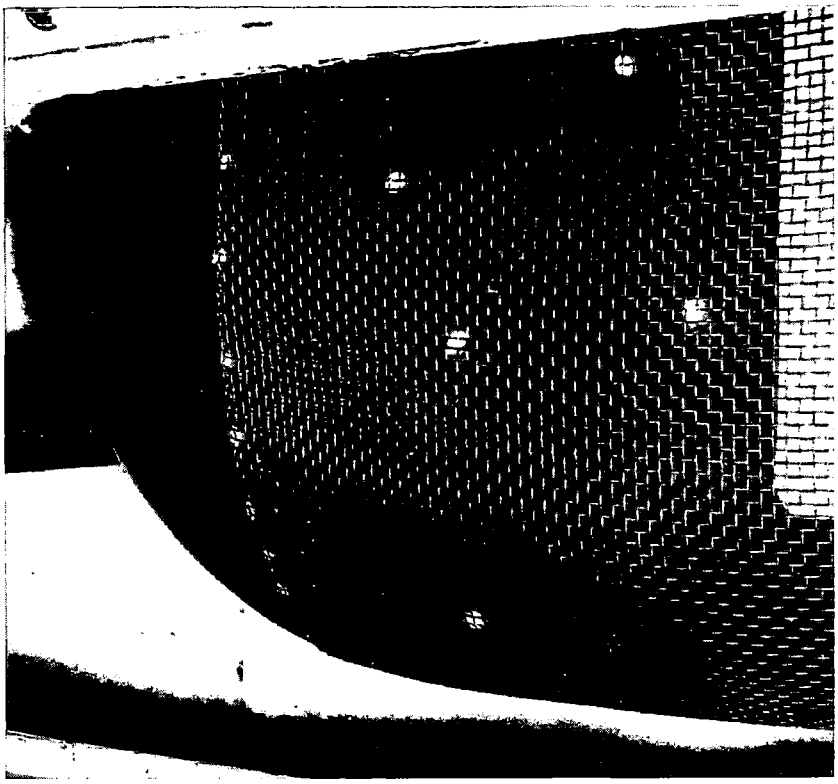

Fig. 11. Wire Meshes Mounted on a Dummy Model.

which were made 0.45 and 0.35 m in breadth respectively. Model No. 720 is a model of a cargo ship with a block coefficient of 0.675, and it is further described in [1]. The velocity distributions of the three models are given on the lower part of Fig. 10.

The velocities are presented in the form $V_A/V_{AN}$, where

$$V_A = \text{local velocity } (=f(r, \theta))$$

$$V_{AN} = \frac{\int_{r_0}^{R} V_{Ar} r dr}{1/2\,(R^2 - r_0^2)} = \text{nominal mean velocity}$$

$$V_{Ar} = \frac{\int_{0}^{2\pi} V_A d\theta}{2\pi} = \text{mean velocity at radius } r$$

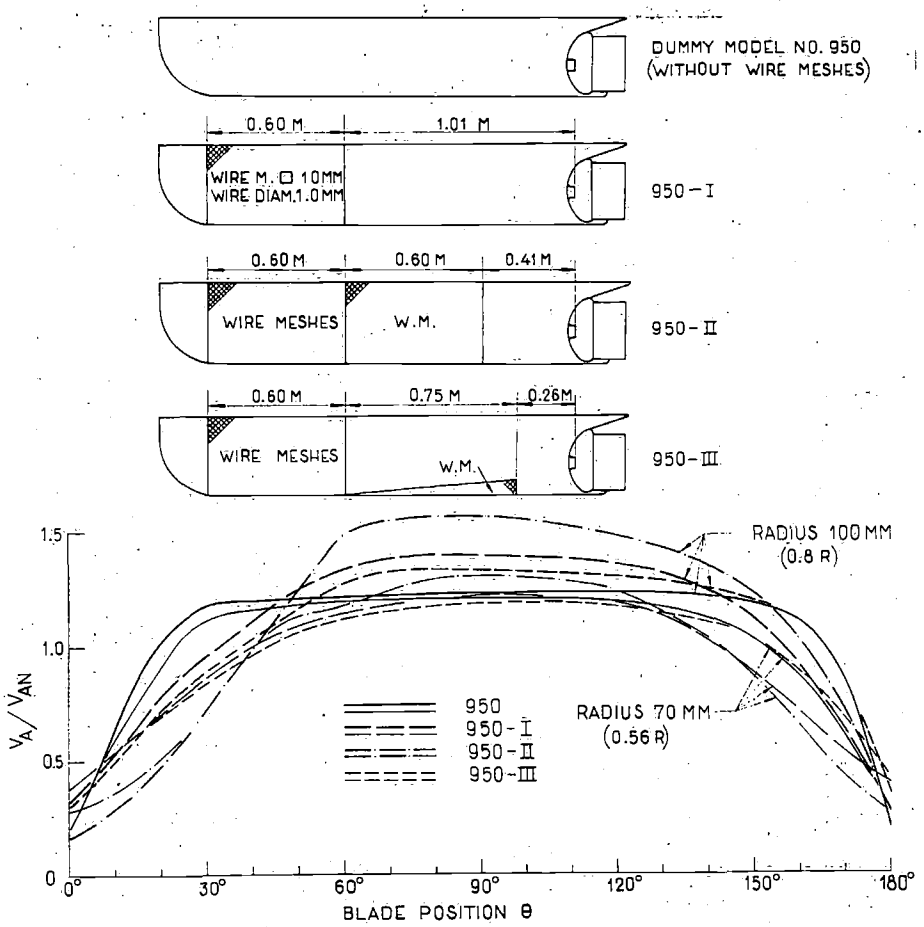


Fig. 12. Different Wire Meshes on Dummy Model No. 950.

$R$=propeller radius=$D/2$

$r_0$=boss radius

As the dummy models are shorter and narrower than the complete ship model, the boundary layer becomes narrower. To compensate for this, wire meshes are mounted flush along the sides of the dummy models, Fig. 11. Dummy No. 950 has been tested with a number of different mesh arrangements, as shown in Fig. 12, where also the corresponding velocity distributions are given. The method used at

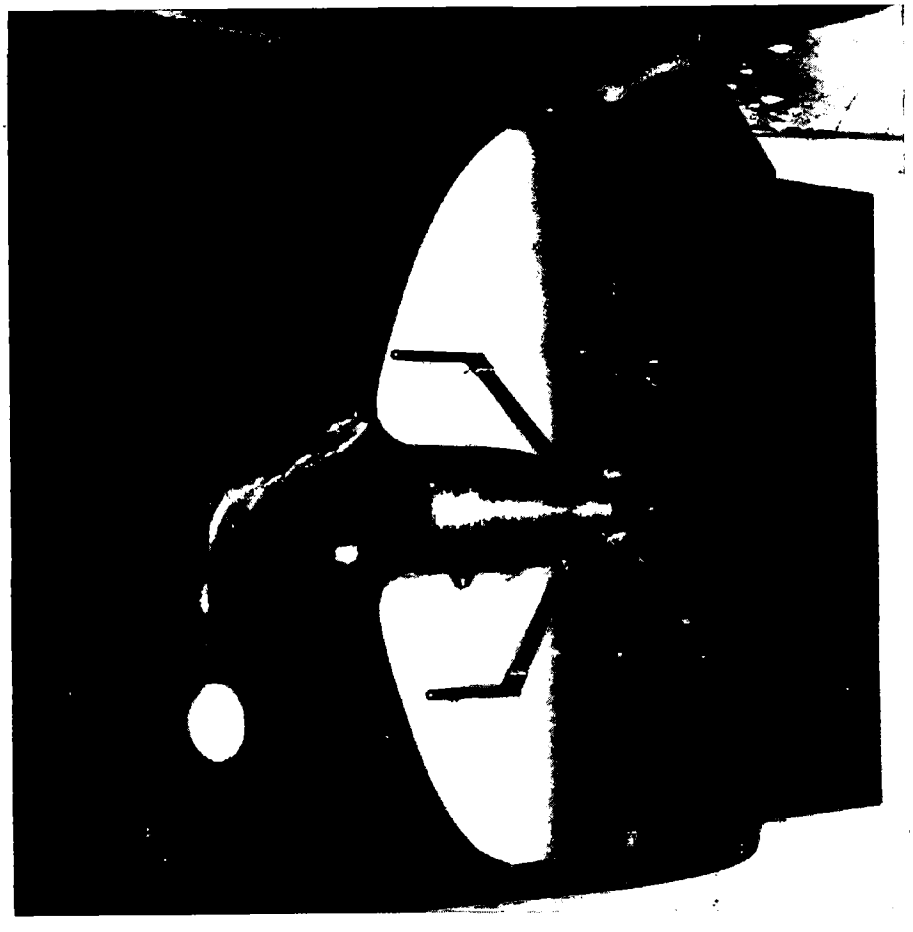

Fig. 13. Pitot Tube Arrangement abaft a Dummy Model.

SSPA for calibrating the distributions abaft the dummy models is illustrated in Fig. 13. A set of four Pitot tubes mounted at different radii on a hub can be fitted to the propeller shaft and turned in the aperture.

Due to the fact that only relatively narrow dummies can be used, only very limited parts are similar to the complete model, Fig. 10. This applies primarily to fuller ships and in some instances it has been necessary to mount transverse wire meshes in addition to the meshes flush along the hull in order to get an approximately correct wake distribution.

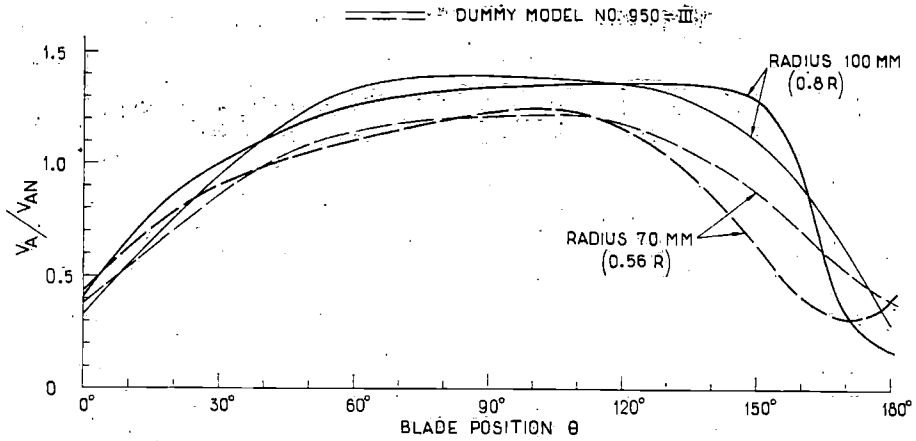


Fig. 14. Velocity Distribution for Ship Model No. 720 and Dummy Model No. 950—III.

## 4. Influence of the Wake Distribution on the Cavitation Patterns

To illustrate the influence of the wake distribution, some results from cavitation tests with propeller model No. P 755 are given. This propeller was designed to operate in the irregular flow abaft model No. 720 (Fig. 1). The design principles are further described in Section 5.

The main dimensions and characteristics of propeller No. P 755 are given in Fig. 21. Complete cavitation tests were performed with this propeller, including thrust and torque measurements, studies of cavitation inception and cavitation patterns in homogeneous flow as well as in different irregular flow distributions.

The caviation tests in irregular flow reported below were carried out in connection with dummy model 950—III (Fig. 12), and the velocity distribution for this model and model 720 are compared in Fig. 14.

Fig. 15 gives a schematic representation of the circumferential variation of the radial cavitation distribution at three different $\sigma$-values and constant $J$, when the propeller operates in the wake distribution 950—III (Fig. 12). The propeller blades pass through the range of high wake behind the stern and the range of low wake in the outer positions, around 90° and 270°. Thus a propeller that is designed for shock-free entrance in relation to the mean inflow velocity will balance between suction and pressure side cavitation. This is clearly indicated in Fig. 15, and by some photographs and

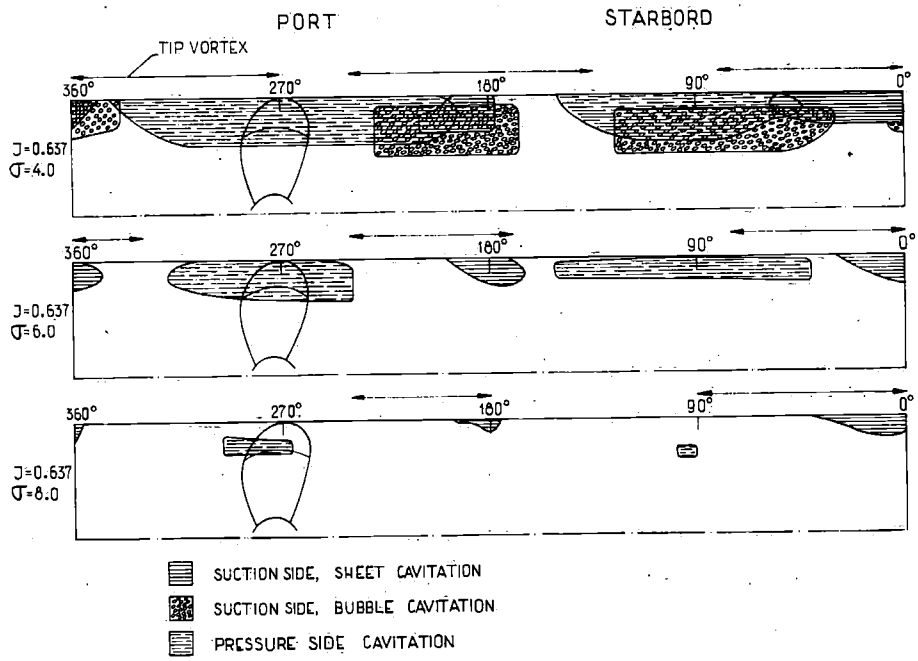


Fig. 15. Circumferential Variation of the Radial Cavitation Distribution for Propeller No. P 755 at $J=0.637$.

sketches representing the 0° and 270° positions, given at the top of Fig. 16. From Fig. 15 it can also be concluded that there is a general tendency for the most extensive suction-side cavitation to occur on the starboard side of the stern and for pressure-side cavitation to be more accentuated on the port side, at about the 270° position. This can primarily be accounted for by the influence of the tangential wake components as explained in Section 3. In addition, a phase lag due to the non-stationary inflow velocity components to the propeller, must be of some importance.

As mentioned in Section 3, a possible method of studying propeller cavitation in non-uniform conditions is to calculate the local $J$- and $\sigma$-values in the positions of interest and test at the corresponding values in homogeneous flow. To illustrate this method, the local speeds of advance in the 0° and 90° positions were calculated, together with the corresponding $J$- and $\sigma$-values, for propeller P 755 in the wake distribution 950—III, Fig. 12. Furthermore the 90° values were corrected for the tangential velocity components in the 90° and 270°

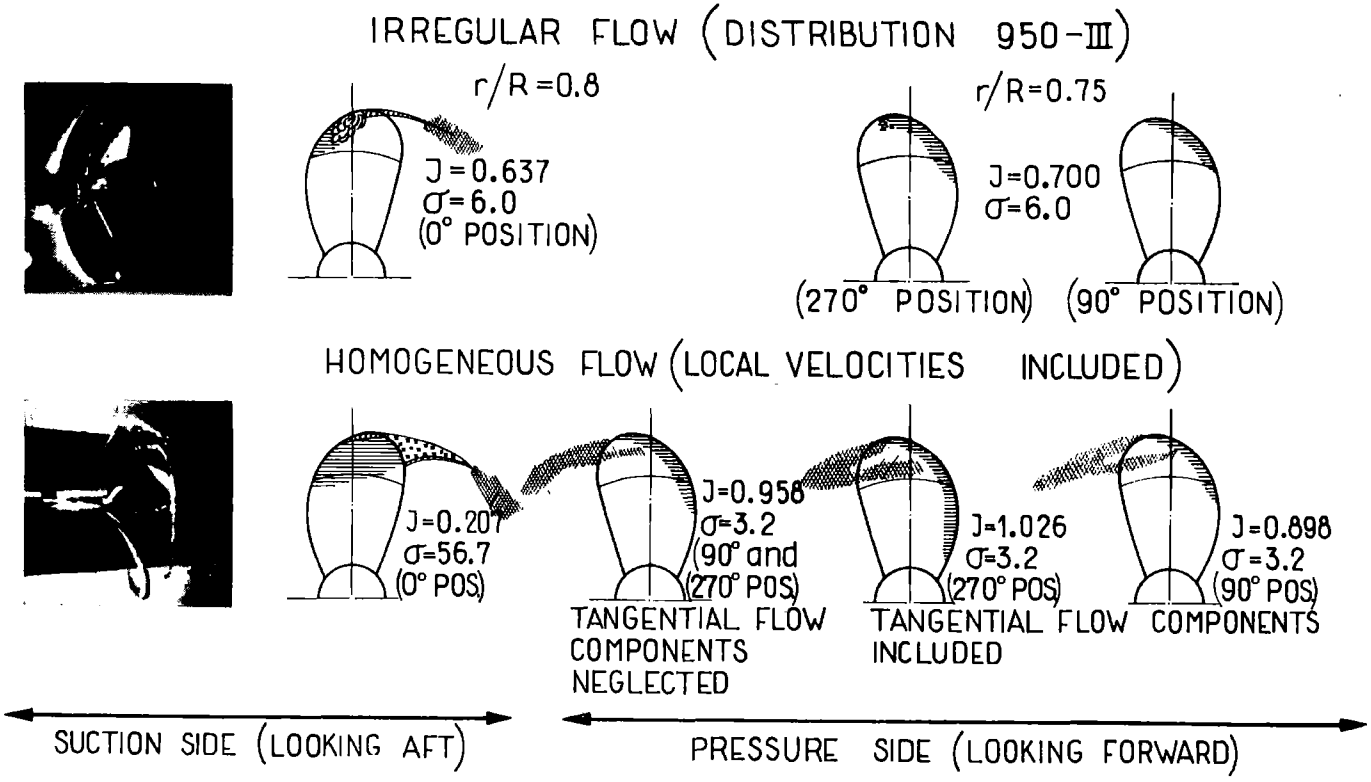


Fig. 16. P 755, Suction-and Pressure-Side Cavitation Patterns in Homogeneous and Irregular Flow.

*Table 1*

| | Loading Condition 1 | | Loading Condition 2 | |
|---|---|---|---|---|
| | $J$ | $\sigma$ | $J$ | $\sigma$ |
| Local velocities calculated for radius | 0.80 $R$ | | 0.75 $R$ | |
| Mean values in irregular flow | 0.637 | 6.0 | 0.700 | 6.0 |
| Local values in 0° position | 0.207 | 56.7 | | |
| Local values in 90° and 270° positions (influence of tangential components ignored) | | | 0.958 | 3.2 |
| Local values in 90° position (tangential components included) | | | 0.898 | 3.2 |
| Local values in 270° position (tangential components included) | | | 1.026 | 3.2 |

positions according to the expressions on page 8 and assuming that the relation between the tangential and axial velocity components $V_T/V_A$ follow the diagram in Fig. 6. The $J$- and $\sigma$-values obtained are summarized in the Table 1.

The relation between the cavitation patterns obtained in the irregular flow and the corresponding spots in homogeneous flow are compared in Fig. 16. It can be concluded that the suction-side cavitation is much heavier in homogeneous flow than in the irregular distribution, which must be explained by influence from the non-stationary inflow velocity components as well as the differences with regard to the blade interference.

The relationship between suction-side cavitation in irregular and homogeneous flow can be further studied in the sketches shown in Fig. 17. To try to find out if an "equivalent velocity" can be defined, at which the cavitation pattern is similar in homogeneous flow and in the top position abaft the stern, three different load conditions have been calculated, assuming different speeds of advance at 0.8 $R$. Fig. 17 shows that the shape of the cavitating region is quite different in homogeneous flow and in a ship wake. In the wake abaft the stern it is primarily located along the leading edge of the blade, whilst in homogeneous flow it is spread over the whole blade tip.

The picture is not so distinct with regard to pressure-side cavitation. From the sketches to the right in Fig. 16 it can be concluded that the influence of the tangential components, *i. e.* the difference between

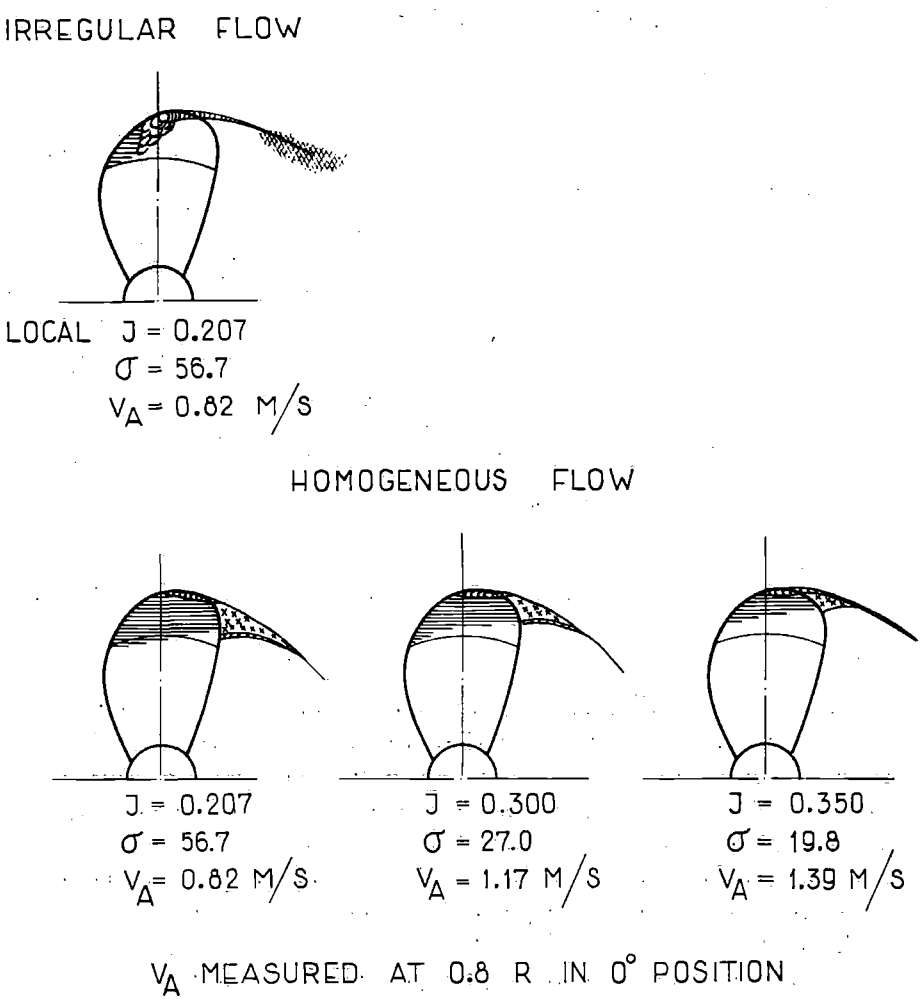


Fig. 17. P 755, Cavitation Patterns in Irregular and Homogeneous Flow.

the cavitating regions in the 270° and 90° positions, is less in the irregular flow distribution than in the corresponding positions simulated in homogeneous flow. This may indicate that the tangential velocity components are smaller abaft the dummy than was assumed in the calculations. In other respects it is difficult to draw any definite conclusions, although it appears as if pressure-side cavitation also becomes exaggerated in homogeneous flow.

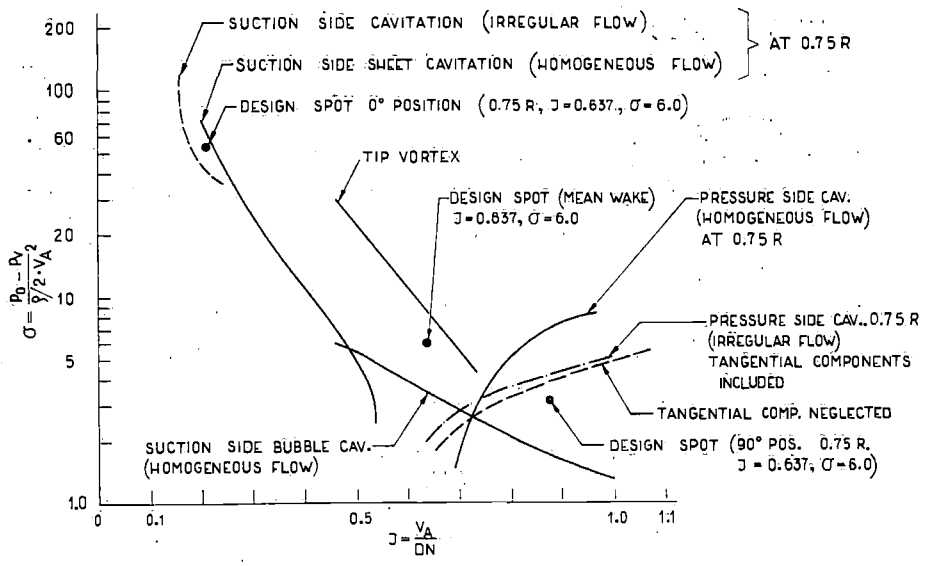


Fig. 18. P 755, Incipient Cavitation Phenomena.

Cavitation inception has been studied in homogeneous as well as in irregular flow. The results are plotted in Fig. 18, where the local $J$- and $\sigma$-values (in 0° and 270° blade positions) have been used to represent the irregular distribution. The differences between the curves for pressure-side cavitation are quite distinct, even where the tangential flow components are taken into account. Both pressure- and suction-side cavitation start earlier (higher $\sigma$-value) in homogeneous than in irregular flow.

To illustrate how sensitive the propeller cavitation patterns are to different wake distributions, propeller No. P 755 has been tested in the distributions abaft 922, which is a broad dummy without wire meshes (Fig. 10), 950 (narrow dummy without wire meshes, Fig. 10) and 950—III (narrow dummy with wire meshes, Fig. 12). The boundary layer of 950 is very narrow, but increases slightly for 922 and considerably for 950—III due to the wire meshes. The wake peak in the top position is most marked for distribution 950.

The results of the cavitation studies are given as photographs and sketches in Fig. 19. Although the wake peak is most marked for 950, the suction-side cavitation is worse for 922 and both suction- and pressure-side cavitation are worst for 950—III. This indicates that

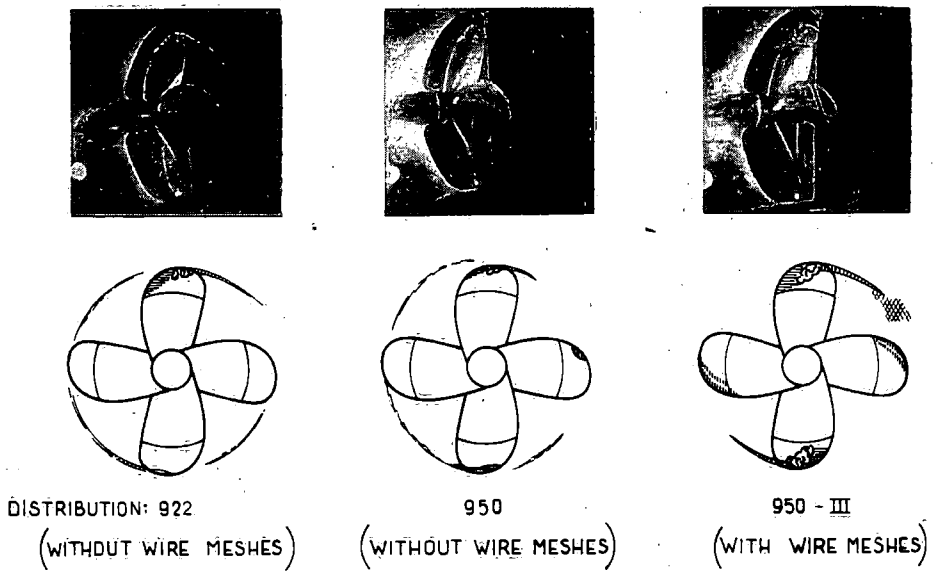


Fig. 19. P 755 in Different Wake Distributions, $J = 0.637$.

the breadth of the boundary layer is a more important factor than the $\Delta w$ value. The increased suction-side cavitation must be explained by the broader wake peak for 950—III, while the increased pressure-side cavitation can be explained by the fact that the effective mean wake is higher and thus also the difference between the mean velocity and the lowest velocity in the 270° position. It must be remembered that the tests were carried out at identical mean $J$-values (*i. e.* identical $K_T$-values). This result also confirms the conclusion above that a cavitation test in homogeneous flow based on the local $J$- and $\sigma$-values does not give the correct picture.

Some of the systematic tests described in Section 5 have been performed with dummy 950—III modified with a wider aperture and spade type rudder, 950—III C Fig. 20. The influence of this modification on the wake distribution was very limited, but nevertheless the influence on the cavitation pattern was quite remarkable, primarily with regard to suction-side cavitation. This is shown in Fig. 20. The reduction in suction-side cavitation obtained in the spade-rudder version primarily has to be explained by the influence of the rudder type and position and the propeller clearances.

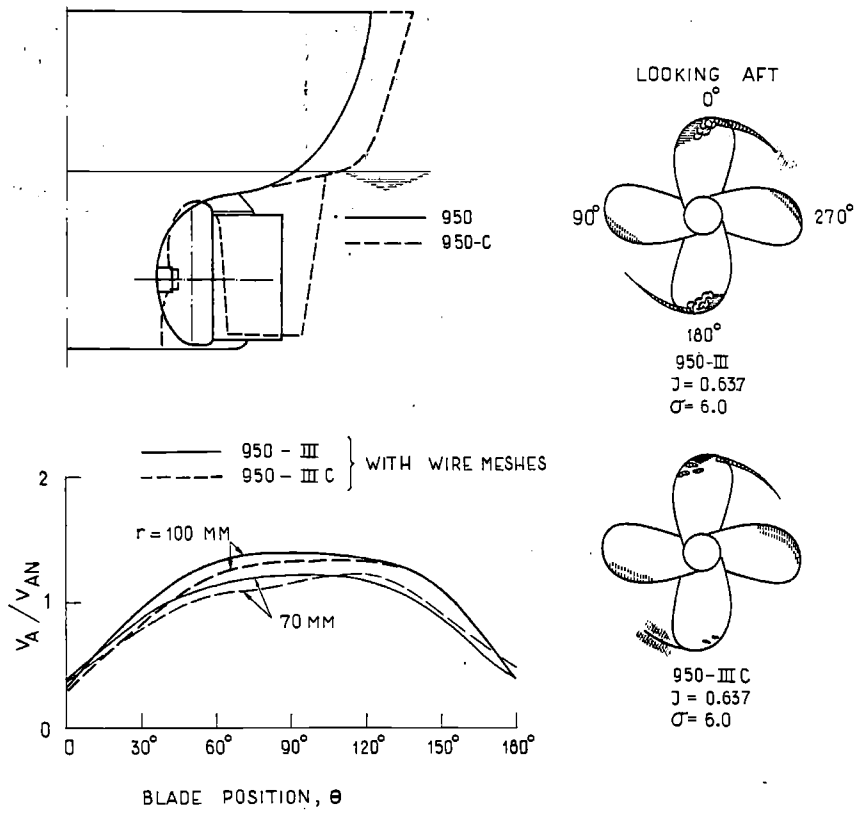


Fig. 20. P 755 in Different Apertures.

## 5. Systematic Tests. Influence of Blade Area Ratio and Profile Shape on the Cavitation Patterns

A comprehensive series of systematic tests has been started at SSPA, primarily to study the influence of different parameters on the cavitation properties of a merchant ship propeller. The results of some of these tests will be summarized below, and the influence of blade area ratio and profile shape especially will be discussed.

*Blade Area Variation*

Propeller model No. P 755 referred to in Section 4, was the parent model in a family of three propellers, Nos. P 754—P 756, with different

*Table 2*

| | |
|---|---|
| *A.* Common design data | $J=0.637$ $K_T=0.193$ $w_T=30\%$ |
| *B.* Wake distribution | $w_r/w_N=2.08-1.61\ x$ (approximately similar to the distribution for model No. 720) |
| *C.* Ideal efficiency, $\eta_i$ | Acc. to KRAMER [12] with empirical correction, $\eta_i=0.97\ \eta_i$ (uncorrected) |
| *D.* "GOLDSTEIN-factor", $\varkappa$ | Acc. to LERBS-TACHMINDJI [13] |
| *E.* Circulation distribution | Optimum wake-adapted, assuming $\mathrm{tg}\beta_i=\frac{1}{\eta_i}\left(\frac{1-w_T}{1-w_r}\right)^{3/4}\mathrm{tg}\beta$ acc. to VAN MANEN [10] |
| *F.* Induced curvature corrections | Taken from [9] approximately similar to GINZEL-LUDWIEG [14] |
| *G.* Friction loss correction | Acc. to [9], partly on mean line curvature and partly on pitch |
| *H.* Profile angle of attack | Hypothesis: Shock-free entrance in relation to the mean speed of advance for each radius |
| *I.* Shape of profile mean lines | Circular |
| *J.* Shape of profile thickness distribution | NACA OOXX – 64 |

blade area ratios. The propellers were designed using the vortex theory as presented in Ref. [9], which in its main features is very similar to the methods described in [10] and [11]. The design principles and data are summarized in Table 2.

The root sections, which are normally determined by strength requirements, were made similar for all the three propellers. The design values of $\sigma$ were $\sigma=8.0$, $\sigma=6.0$ and $\sigma=4.0$. The outer sections were designed to be free from cavitation above $\sigma=6.4$ $(=8\cdot 0.8)$, $\sigma=4.8$ $(=6\cdot 0.8)$ and $\sigma=3.2$ $(=4\cdot 0.8)$ for propellers Nos. P 754, P 755 and P 756 respectively. The security factor 0.8 has been used frequently as an allowance for irregular flow influence and scale effects. The main dimensions and data of the three propellers are given in Fig. 21.

The open-water test results are shown in Fig. 22, together with curves illustrating incipient cavitation phenomena in homogeneous flow. The $K_T$-curves agree satisfactorily with the design spot, except for P 756 which gave too high $K_T$-value. The general impression from the test results was that the margin against $K_T$ and $K_Q$ breakdown is

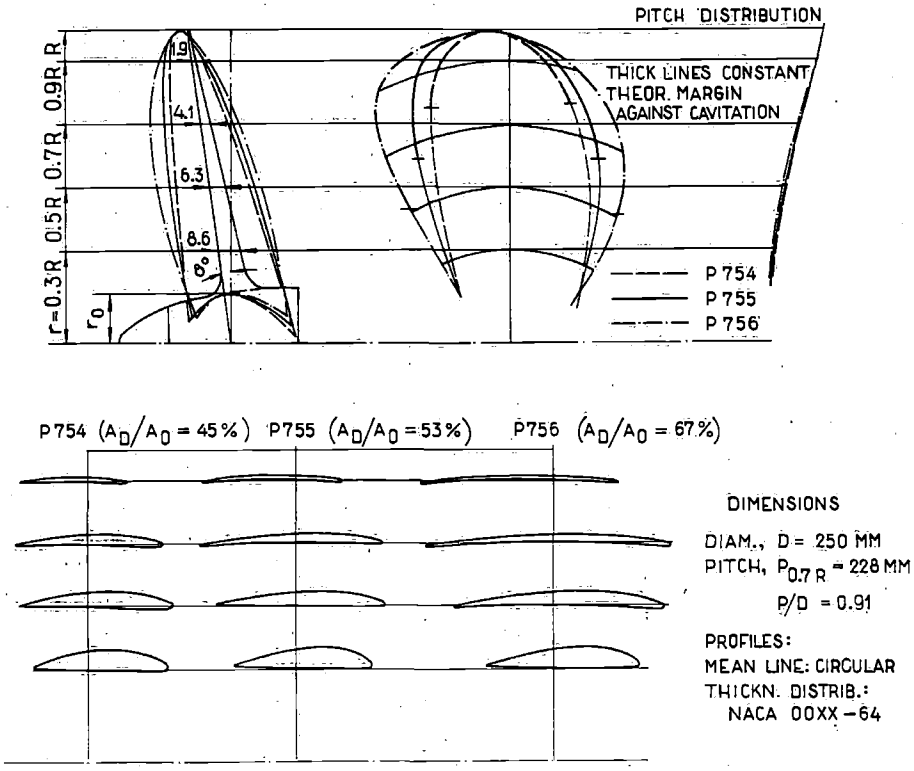


Fig. 21. P 754—P 756, Main Dimensions.

large in homogeneous as well as in irregular flow, although as could be expected it is slightly smaller for the irregular case. The margin against incipient suction-side cavitation in homogeneous flow at 0.75 $R$ is more than 35% (*i. e.* $\sigma_{Design}/\sigma_{Incept.} > 1.35$) for all the propellers. However tip vortex cavitation starts at much higher $\sigma$-values.

A well-known cavitation criterion has been proposed by BURRILL [15]. His presentation is used in Fig. 23, where also the design spots, $\sigma=8$, 6 and 4 for propellers Nos. P 754, P 755 and P 756 respectively have been plotted. These spots are parallel to BURRILL's line but well above this line as well as the Wageningen line [16] also given.

The cavitation patterns in irregular flow (950—III) have been studied at three loadings corresponding to $\sigma=8$, 6 and 4 and at the design value of $J=0.637$ for each propeller. These spots are plotted in Fig. 23 and the cavitation pictures are shown in Fig. 24 in the form

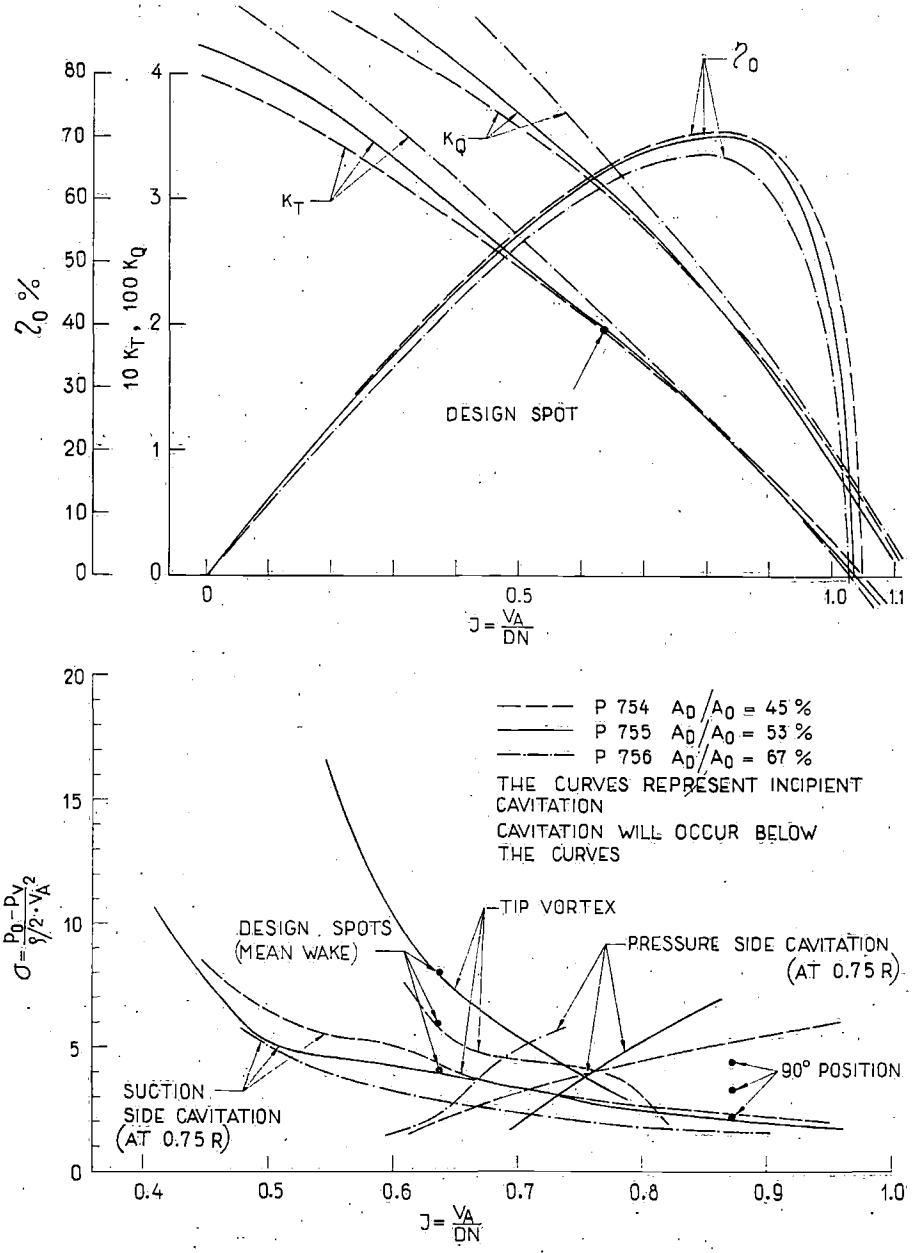


Fig. 22. P 754–P 756; Open Water Test Results and Incipient Cavitation in Homogeneous Flow.

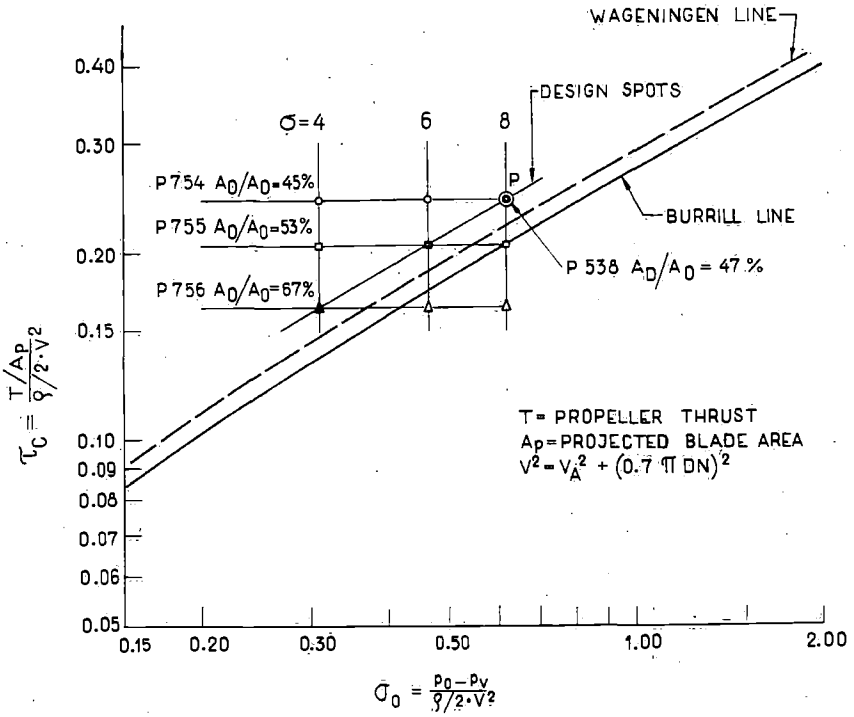


Fig. 23. Cavitation Criteria.

of photographs and sketches with the blades in the 0°, 90°, 180° and 270° positions.

In the design spots, ($\sigma$=8, 6 and 4 for propellers Nos. P 754, P 755 and P 756 respectively) the extent of suction-side cavitation is fairly similar for all the propellers, *i. e.* heavy tip vortex with sheet cavitation at the leading edge near the tip when the blades pass the stern. On the pressure-side sheet cavitation occurs near the leading edge in the outer blade positions. For the three spots above the design spots in Figs. 23 and 24, the cavitation is heavier and bubble cavitation appears on the suction side in the top and bottom positions. This type of cavitation is assumed to be most dangerous from the erosion point of view. The connection between model cavitation patterns and ship propeller erosion will be further considered in Section 6.

For comparison a conventional propeller of the Wageningen B-series type has been tested. This propeller, No. P 538, has a blade area ratio of 47% and thus slightly larger than P 754. The pitch ratio is 0.95 and

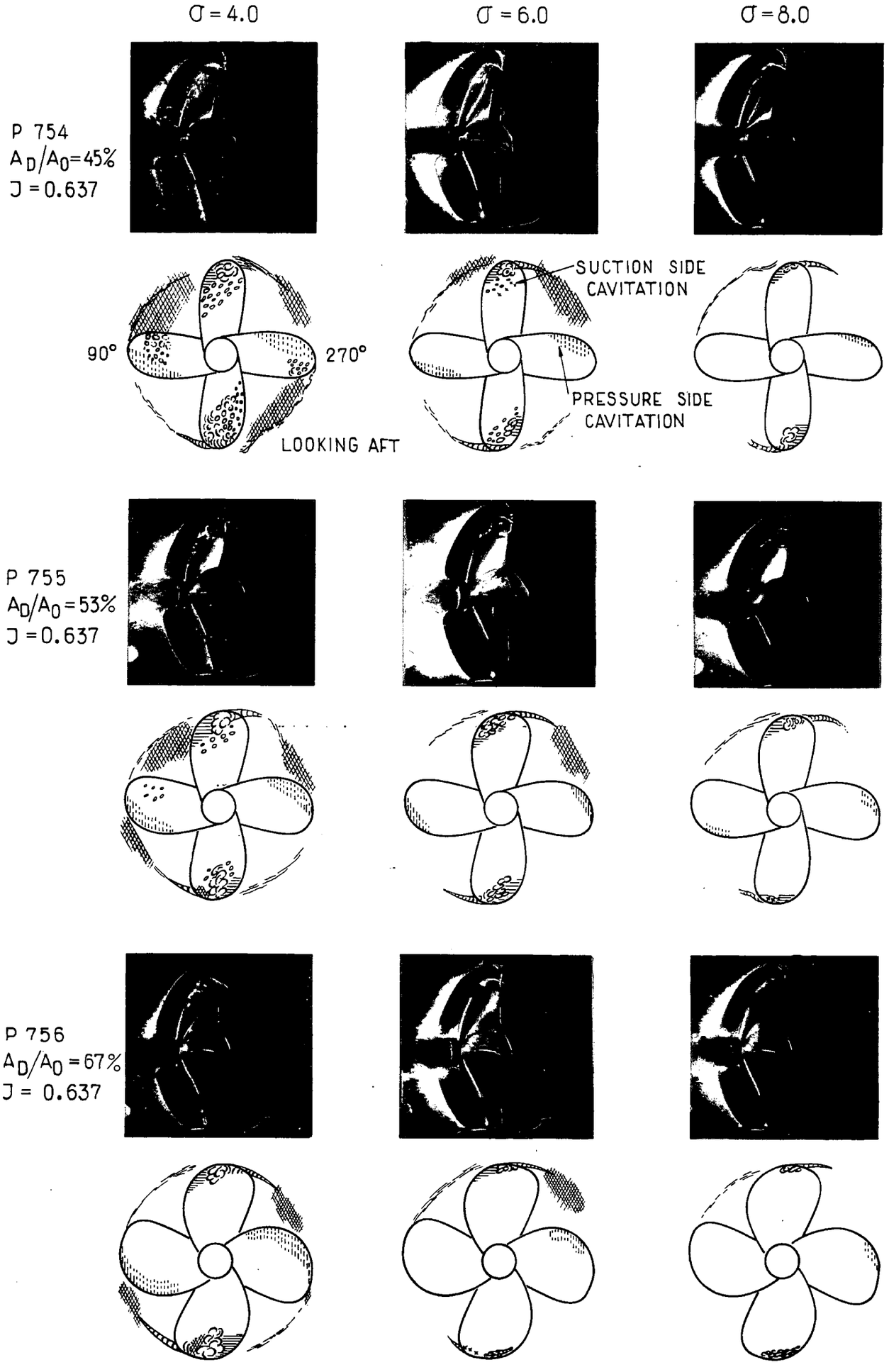


Fig. 24. P 754—P 756, Cavitation Patterns in Distribution 950—III.

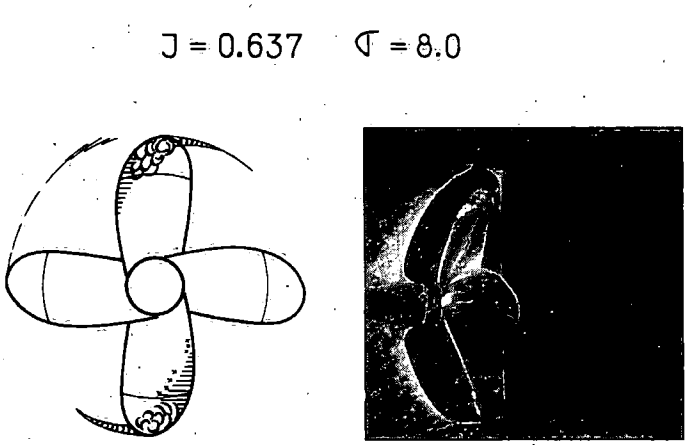


Fig. 25. P 538, Cavitation Patterns in Distribution 950—III.

$K_T=0.200$ for $J=0.637$ which is very similar to the design spot for the propellers P 754—P 756. The cavitation picture at $\sigma=8$ in the distribution 950—III is given in Fig. 25. The suction-side cavitation is much heavier than for P 754 but it is completely free from pressure-side cavitation, which indicates that it operates at a larger positive angle of attack. It is interesting to note that although the cavitation is rather violent, the load condition ($\sigma=8.0$) is quite normal, *i. e.* fairly close to BURRILL's line in Fig. 23.

Diagrams of cavitation inception (Fig. 22) for the three propellers, P 754—P 756, seem to indicate that the propellers operate at a positive angle of attack at the design $J$. An analysis of the open-water test

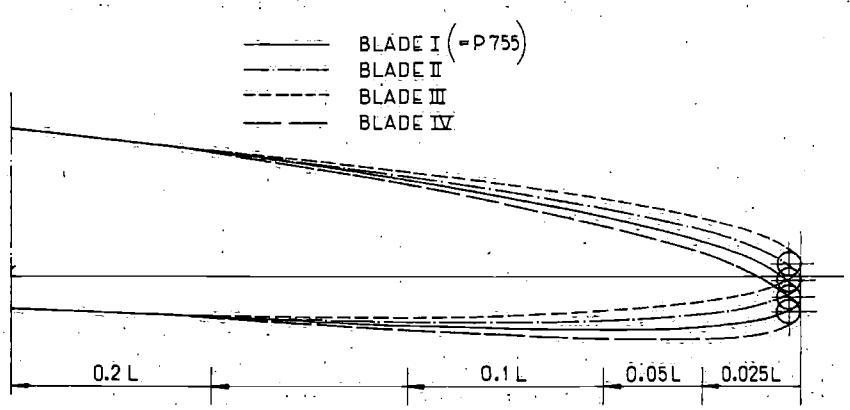


Fig. 26. P 933, Profile at 0.7 $R$.

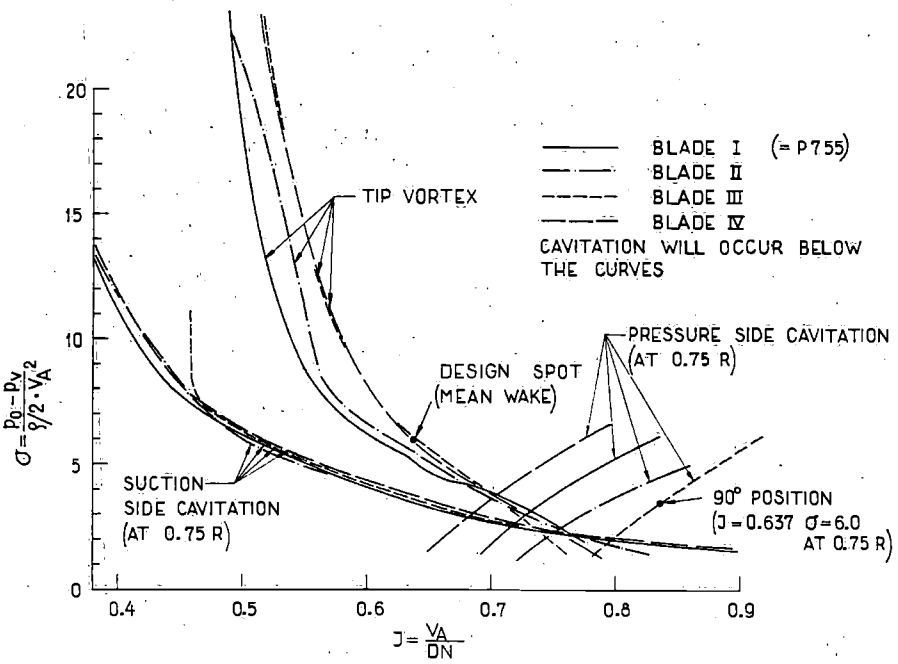


Fig. 27. P 933, Incipient Cavitation in Homogeneous Flow.

results with the equivalent profile method shows the same trend. Nevertheless pressure-side cavitation occurs over a large part of the revolution (see Fig. 15). Experience of full-scale propellers has shown that this type of cavitation has frequently resulted in pressure-side erosion. Different methods of eliminating the pressure-side cavitation were therefore investigated. The results of these experiments are given below.

*Profile Shape Variation*

Three series of experiments are reported namely: —

*a*. Systematic variation of the curvature of the forward part of the profile mean lines
*b*. Systematic variation of the leading edge radius
*c*. Systematic variation of the profile thickness distribution

The first two variations were based on the parent form, P 755. Two new propellers, Nos. P 933 and P 952, were manufactured with slight differences on the leading edge of the blades from 0.5 $R$ to the tip according to Figs. 26 and 29 respectively.

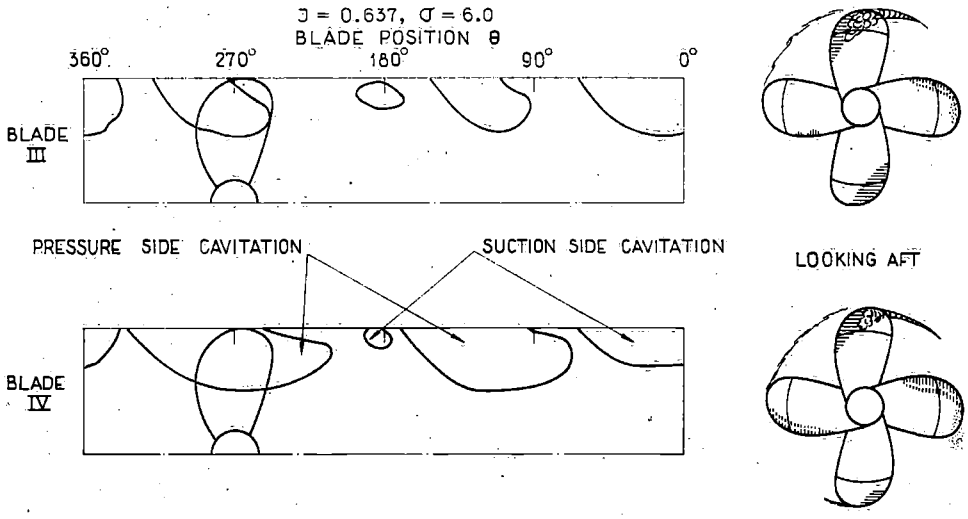


Fig. 28. P 933, Blades III and IV, Circumferential Variation of the Cavitation Distribution at $J=0.637$.

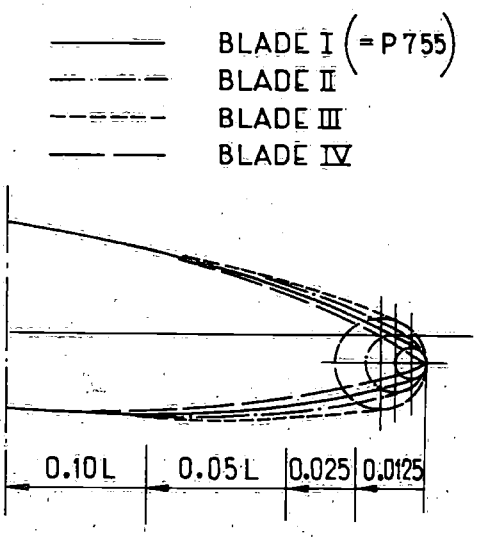


Fig. 29. P 952, Profiles at 0.7 $R$.

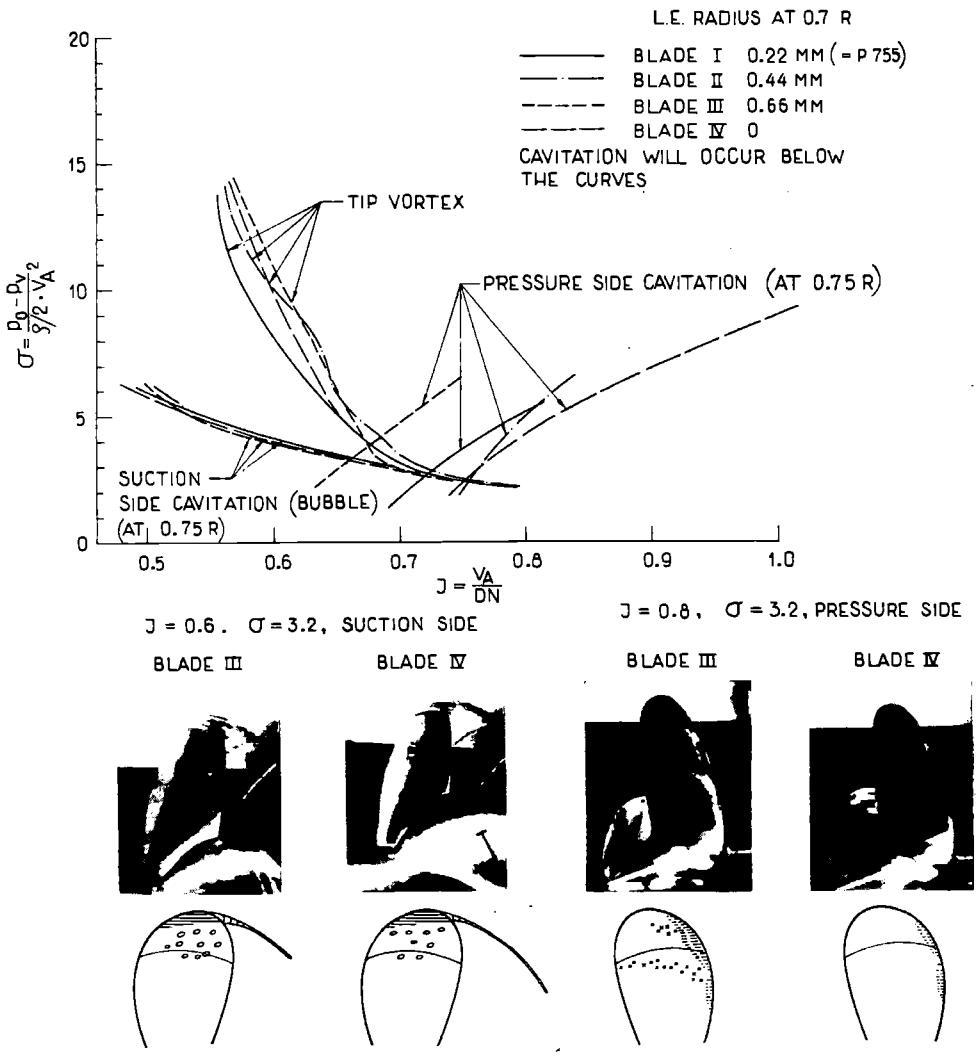


Fig. 30. P 952, Incipient Cavitation.

The results of the tests with propeller P 933 are given in Figs. 27 and 28. In Fig. 27 the results of studies of incipient cavitation at 0.75 $R$ in homogeneous flow are given. The influence of the modifications with regard to suction-side cavitation is neglible, whilst there is a distinct influence on the pressure-side cavitation. The profile for which the mean line is most flattened out gives the best results. This

*Table 3*

| | |
|---|---|
| *A*. Common design data | See Table 2 |
| *B*. Wake distribution | See Table 2 |
| *C*. Ideal efficiency, $\eta_i$ | Acc. to SCHULTZ [17] |
| *D*. "GOLDSTEIN-factor", $\varkappa$ | Acc. to TACHMINDJI [18] |
| *E*—*F*. | See Table 2 |
| *G*. Friction loss correction | Applied as a pitch correction |
| *H*. | See Table 2 |
| *I*. Shape of profile mean line | NACA $a=0.8$ |
| *J*. Profile thickness distribution | See text below |
| *K*. Empirical pitch correction | 1% increase |

is further illustrated in Fig. 28 which shows the circumferential variations of the radial cavitation distribution at $J=0.637$ and $\sigma=6.0$ for the extreme blades, III and IV in distribution 950—III. The modifications were, however, not sufficient to eliminate the pressure-side cavitation.

The results of the tests with propeller No. P 952 are illustrated in Fig. 30. The variation of the leading edge radius has no significant influence on the inception of suction-side cavitation at 0.75 $R$. The influence on incipient pressure-side cavitation is more distinct, however, and the largest leading edge radius gives noticeably the worst results. Unfortunately no tests with this propeller in an irregular flow distribution are yet available. The sketches and photographs given in the lower part of Fig. 30 illustrate the differences between the two extreme blades at some extreme load conditions in homogeneous flow.

Since the design of the propellers Nos. P 754—P 756, new information of value for the design work has become available. Primarily, new diagrams of the ideal efficiency, $\eta_i$, and the "GOLDSTEIN-factor", $\varkappa$ have been worked out [17, 18] and the influence of the boss diameter can thereby be determined. When preparing the next systematic series of propellers, Nos. P 905—P 907, which included a variation of the thickness distribution of the profiles, this new information was used. The design principles and data were those given in Table 3.

The shape of the profile thickness distribution, item *J*, was: —

NACA 66 (modified) for propeller No. P 905

NACA OOXX-64 for propeller No. P 906

NACA 16—for propeller No. P 907

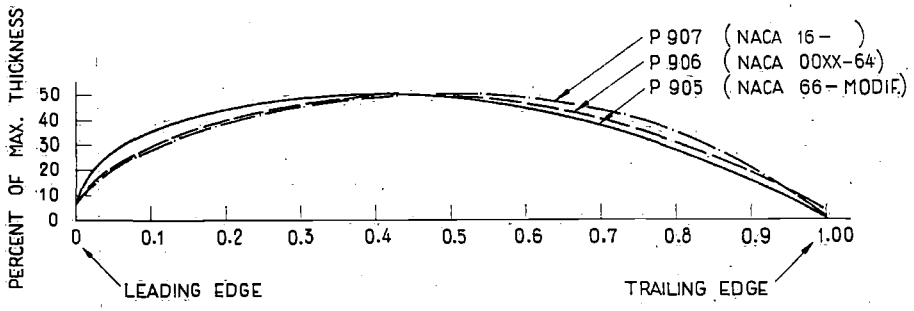


Fig. 31. P 905—P 907, Profile Thickness Distributions.

The different distributions are illustrated in Fig. 31. Small modifications in the thickness of the trailing edge had to be applied to the profiles for practical reasons. The blade contour was made similar to propeller P 755, Fig. 21. The main particulars of propeller models Nos. P 905—P 907 are: —

| | |
|---|---|
| Number of blades=4 | $P/D$ =0.936 |
| Diameter $D$ =0.250 m | $A_D/A_O$=53% |
| Pitch (0.7 $R$) $P_{0.7}$=0.234 m | Rake =8.0° |

The open-water test results are compared in Fig. 32. All the $K_T$-curves fall slightly below the design spot, despite the fact that an empirical increase of 1 % had been added to the pitch (Table 3).

The propellers have been compared on the basis of: —

1. Efficiency in open and behind conditions
2. $K_T$- and $K_Q$-decrease in homogeneous and irregular flow
3. Incipient cavitation in homogeneous flow
4. Cavitating regions in homogeneous and irregular flow.

The self propulsion tests were carried out in conjunction with ship model No. 720. Unfortunately the dummy model version 950—III, was not available at the time for the cavitation tests. As mentioned in Section 4, they were instead carried out behind dummy model version 950—IIIC. The two dummy models are compared in Fig. 20 together with some cavitation test results obtained with propeller P 755.

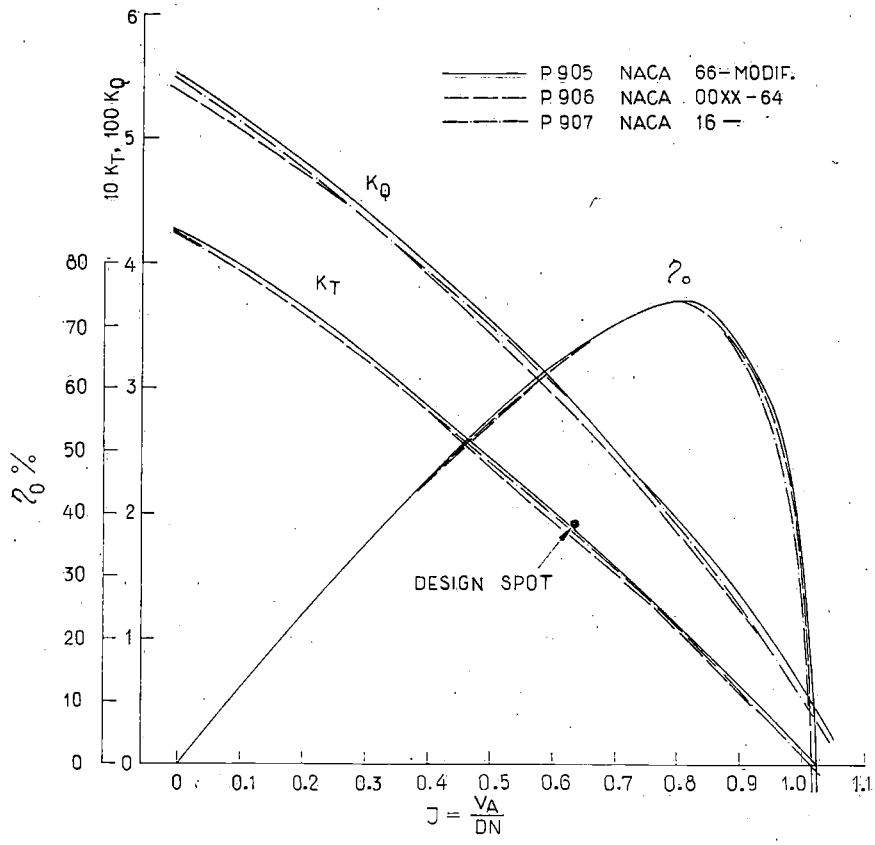


Fig. 32. P 905—P 907, Open Water Test Results.

Some results illustrating item 1 above have been summarized in Table 4. For comparison, propeller model P 755 has also been included.

No significant conclusions can, however, be drawn from this table. The only remarkable feature is the relatively low $\eta$-value obtained with P 907. This result does not correspond to a low $\eta_0$-value in the open condition and possible explanations are small differences in the model conditions, REYNOLDS number effects and inaccuracies in the measurements.

The conclusion with regard to item 2 ($K_T$- and $K_Q$-decrease) is that no influence could be established in homogeneous or irregular flow at the design spot. At the extremely low spot, $\sigma=3.2$ and $J=0.5$, and in homogeneous flow, thrust- and torque-decreases could be established

*Table 4*

| Propeller | Self propulsion tests at design speed (16.5 knots) | | Open Water tests at design $J=0.637$ | |
|---|---|---|---|---|
| | $N_S$ | $\eta=P_E/P_S$ | $K_T$ | $\eta_0$ |
| No. | r/min. | % | | % |
| P 905 (NACA 66−) | 109.6 | 76.5 | 0.187 | 66.3 |
| P 906 (NACA OOXX−64) | 111.1 | 76.0 | 0.180 | 66.1 |
| P 907 (NACA 16−) | 111.4 | 74.6 | 0.186 | 66.2 |
| P 755 (Old design. NACA OOXX−64) | 108.4 | 75.1 | 0.193 | 64.2 |

for all the propellers, as given in Table 5. The decrease is lowest for P 905, but fairly similar for all the propellers.

Incipient tip vortex cavitation and suction- and pressure-side cavitation at 0.75 $R$ have been illustrated in Fig. 33. It is surprising to note that all the lowest curves belong to P 906. The design spot, $J=0.637$ and $\sigma=6.0$, is illustrated in Fig. 34. The spot corresponding to the local $J$- and $\sigma$-values in the 90° position (tangential components ignored) has been plotted. Although according to this spot, propeller P 907 should cavitate, none of the propellers shows any sign of pressure-side cavitation. This is in agreement with the conclusion above that the danger for cavitation is less in irregular than in homogeneous flow.

*Table 5*

$\sigma=3.2$ $J=0.5$

| Propeller | Decrease with regard to | |
|---|---|---|
| | $K_T$ | $K_Q$ |
| No. | % | % |
| P 905 | 27 | 25 |
| P 906 | 32 | 25 |
| P 907 | 34 | 25 |

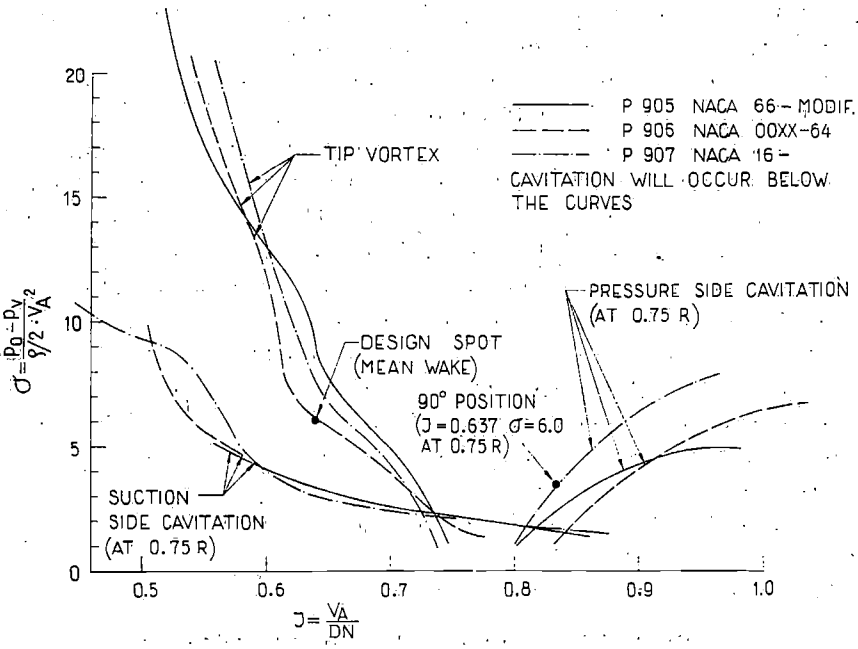


Fig. 33. P 905—P 907, Incipient Cavitation in Homogeneous Flow.

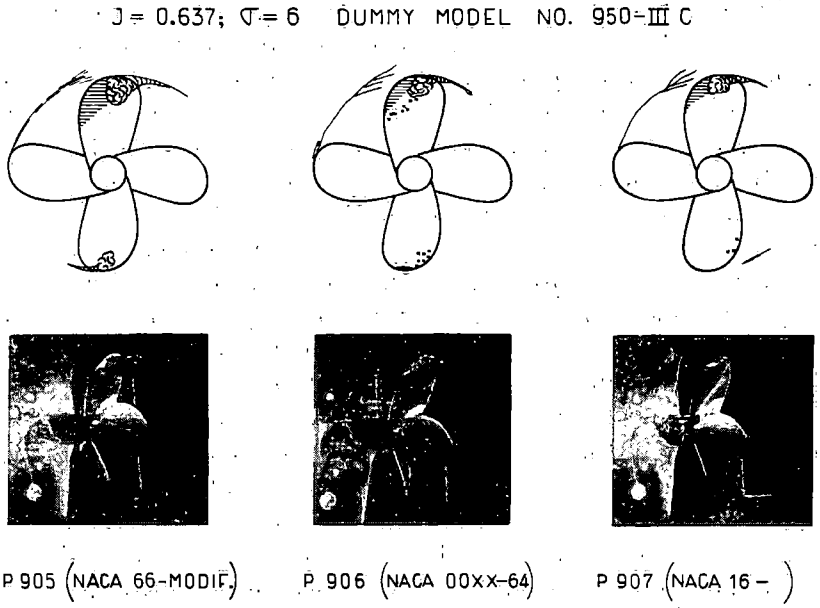


Fig. 34. P 905—P 907, Cavitation Patterns at $J=0.637$, $\sigma=6.0$.

On the basis of the results reported, none of the thickness distributions tested shows any significant superiority. The propellers P 905—P 907 are more or less equivalent from all the aspects considered.

Propeller No. P 755 cavitated along the leading edge at the design spot, when tested abaft dummy 950—III C, Fig. 20. Slight improvements were obtained from this point of view if the forward part of the mean line was flattened out (P 933 blade III) or if the leading edge was sharpened (P 952 blade III). None of these alternatives was, however, sufficient to eliminate pressure-side cavitation. Propellers Nos. P 905—P 907, which were in some respects designed according to different principles (Table 3), are completely free from pressure side cavitation at the design spot. On the other hand, as could be expected, suction-side cavitation starts at higher $\sigma$-values than for P 755. This however, does not correspond to a significantly worse cavitation picture in the top position at the design spot, as might be concluded when comparing Fig. 34 and the corresponding sketches in Fig. 24.

## 6. Scale Effects and Ship-Model Correlation

Different reasons for scale effects arising when testing propeller models in irregular flow in a cavitation tunnel, have been mentioned in the preceding Sections. These include the difficulties in simulating the irregular flow distribution desired, lack of knowledge with regard to the wake distribution for a ship, unknown REYNOLDS number effects and wall effects in the cavitation tunnel. Many other important reasons can be mentioned. Too little is known about the influence of the state of the water on the cavitation phenomena. The effect of entrained and dissolved gases as well as the influence of the degree of turbulence must be further studied. Basic research work, as well as more experience from model and full scale experiments, is required.

New problems arise with regard to the question of full scale information. Complete ship propeller cavitation experiments, including the recording of the cavitation patterns, studies of cavitation inception and thrust- and torque measurements are for practical reasons difficult and expensive. Results of this type are so far available only for warship propellers. At present, most of the information on full scale cavitation must be gathered from the studies of propeller erosion patterns. Such studies are, however, complicated by difficulties in separating cavitation erosion from different types of corrosion and by difficulties in

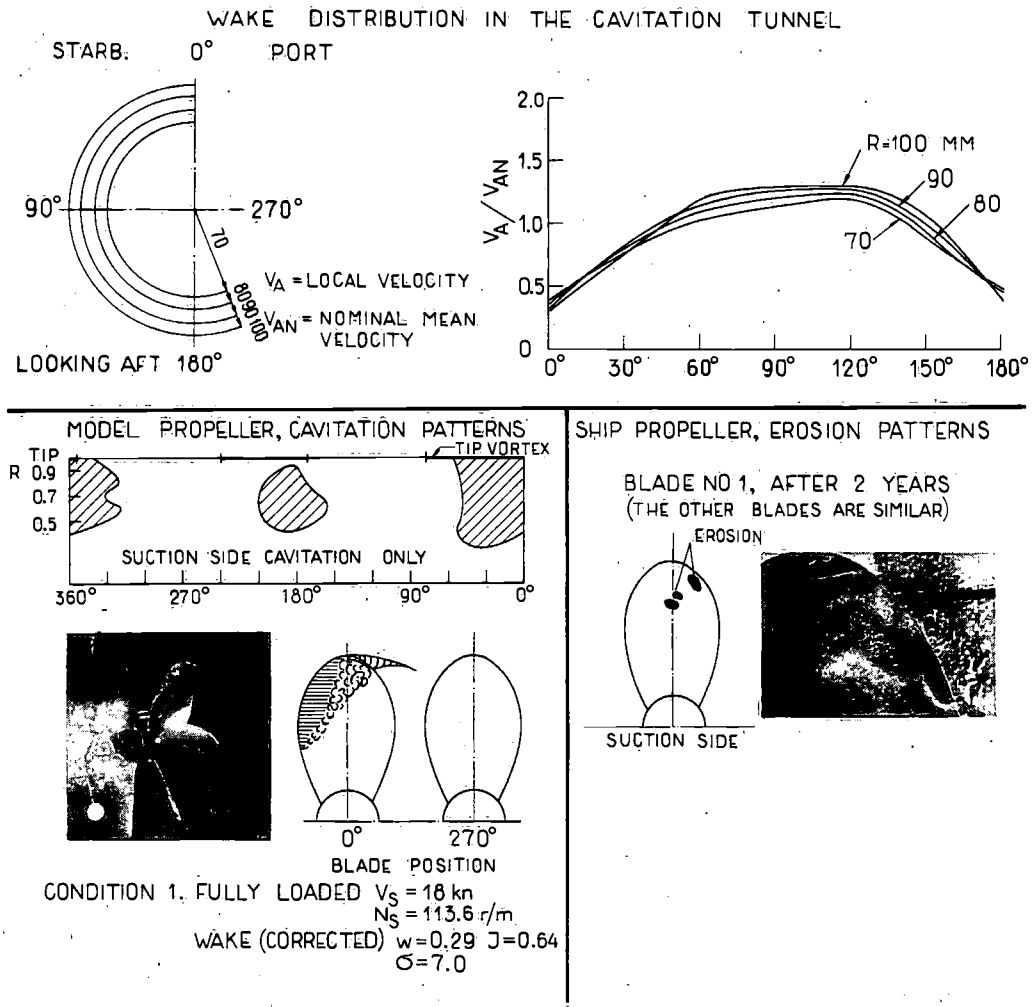


Fig. 35. Comparison Model-Ship Propeller.

finding the relation between erosion patterns and cavitation pictures. Perhaps the technique of using rapidly eroding material in the model tests [19] will give valuable information on the types of cavitation that cause erosion and to what extent cavitation can be tolerated.

At SSPA an extensive programme is in progress for studying erosion patterns on full-scale propellers and comparing them with cavitation pictures from model tests. Some examples from this work will be given.

Fig. 35 is an example of a propeller which after about two years

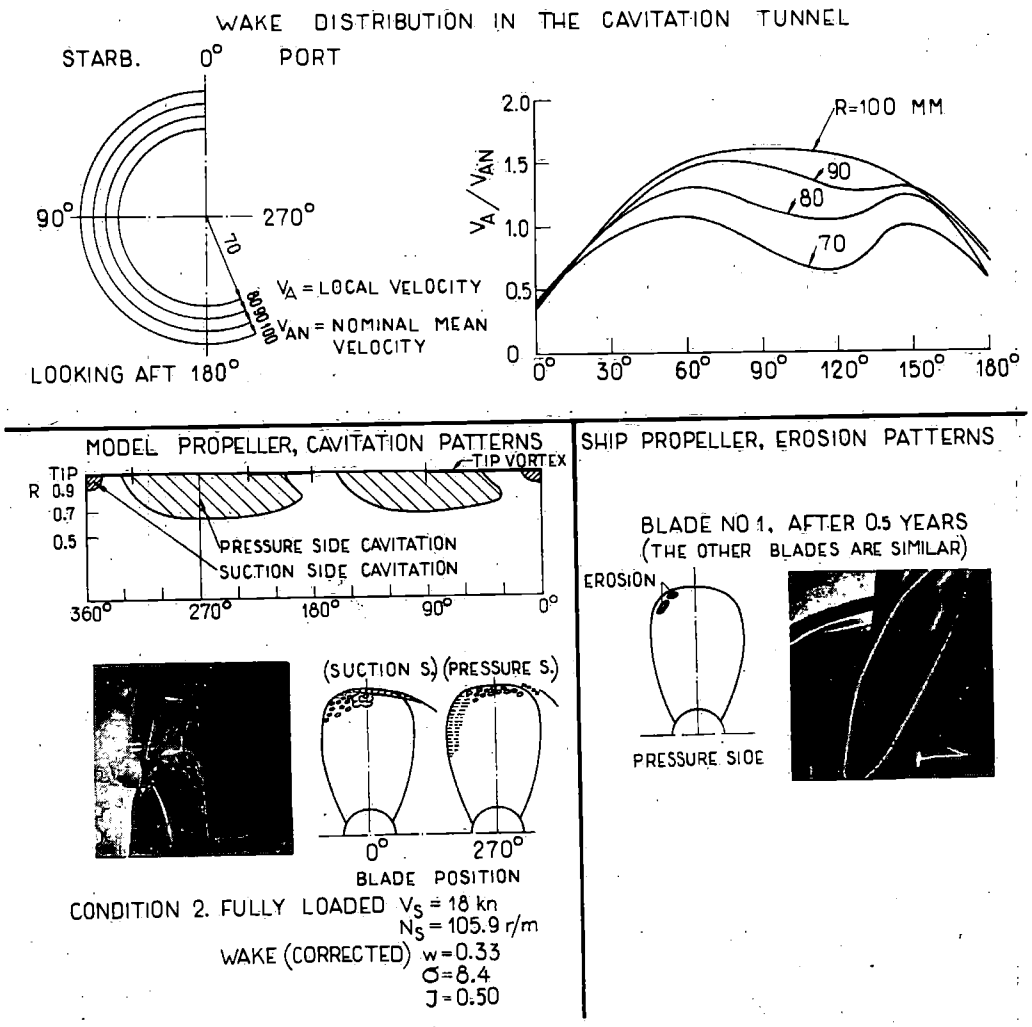


Fig. 36. Comparison Model-Ship Propeller.

showed clear signs of suction-side erosion near the trailing edge on all the blades. The propeller model has been tested in a wake distribution which can be expected to be fairly representative of the actual ship. The distribution is shown on the top of Fig. 35. To the left the cavitation pictures from the model experiments are given. Only one $J$-$\sigma$-condition corresponding to the ship wake is presented (see Section 3). The difference between model and ship wake was regarded very small.

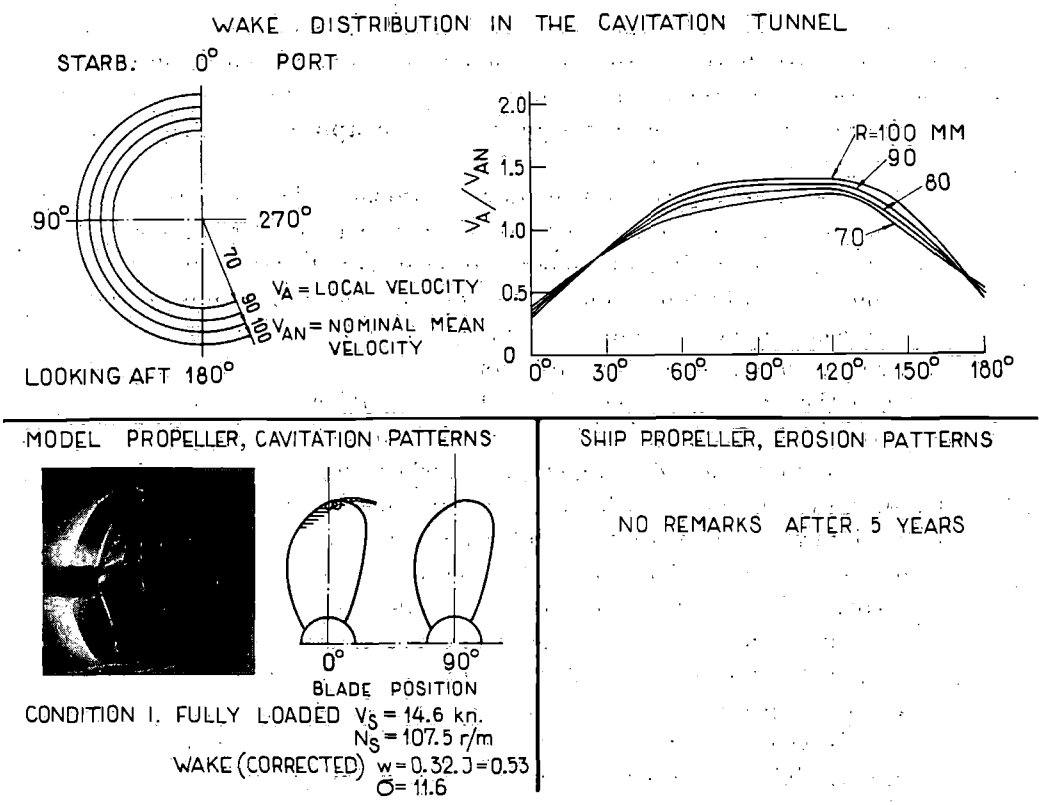


Fig. 37. Comparison Model-Ship Propeller.

To the right some pictures from the full scale propeller are shown. The regions of damage correspond fairly well to the downstream parts of the regions of heavy suction-side cavitation registered at the model tests.

The next example is a propeller which had sustained damage near the leading edge of the pressure side. Model tests were carried out in a representative wake distribution, shown on the top of Fig. 36. The damage on the pressure-side, illustrated to the right of the figure, corresponds to pressure-side cavitation in the model tests (left on Fig. 36) in the 90° position. On the other hand it is surprising to note that the tip cavitation on the suction side, which is rather heavy, has not resulted in any visible erosion. A possible explanation is that the cavitation disappears into the tip vortex so that no implosion takes

place on the blades. Furthermore, as is illustrated on the diagrams of the radial distribution of the cavitation at different angular positions, the suction-side cavitation is limited to a very limited region abaft the stern, whilst the pressure-side cavitation appears over a much larger part of the revolution.

The last example (Fig. 37) refers to a propeller design, which has not shown any sign of visible erosion after several years in service on different sister ships. The model propeller is not free from cavitation, but the cavitation is confined to the parts near the blade tip and can be regarded as very limited tip-vortex cavitation. It is also limited to a very local region in the 0° position.

From the above examples, as well as a number of similar results available, it can be concluded that the model tests undoubtedly give some indication of danger of propeller erosion. On the other hand, many difficulties still exist when evaluating the model cavitation pictures and predicting full-scale behaviour. In some cases contradictory results have been obtained and it is especially difficult to explain why in some instances no full-scale erosion damage is visible although the model propellers indicate heavy cavitation. Of course, the material used can be an important factor.

Another experience is that it seems as if fairly small modifications on a ship propeller can in some cases modify the cavitation picture quite radically. This has also been reported by Pascault [20], who found that a 2.6% decrease of the pitch of a propeller which had shown suction-side erosion caused pressure-side cavitation to occur instead

## 7. Summary and Conclusions

The problem of propeller cavitation in irregular flow is very complicated and the experimental methods available all have their advantages and drawbacks. Much research work is needed for a good understanding of all the different aspects. Some interesting conclusions can, however, be drawn from the investigations reported in the present paper and will be summarized below: —

1. The circumferential variations of the wake increase with ship fullness and are very large for a twin-screw tanker (Fig. 4).
2. The tangential velocity components can not be neglected in cavitation tests. The influence can be established with the SSPA dummy models.

3. Difficulties arise when using afterbody dummies in a limited test section of the size used at SSPA, primarily due to the danger of separation of the flow. This limits the possible breadth of the dummy models.
4. Tests in homogeneous flow at correct local $J$- and $\sigma$-values can not be used to simulate the cavitation picture in the irregular flow abaft a ship model.
5. The breadth of the wake peak abaft a dummy model is of importance. When comparing two wake distributions, maximum wake abaft the stern does not necessarily correspond to maximum suction-side cavitation.
6. For the propellers studied, the suction-side cavitation was very limited at loadings below BURRILL's line (Fig. 23) and up to the design spots it was reasonable. Above the design spots (*i. e.* at lower $\sigma$) bubble cavitation appeared on the suction side. All the propellers in the blade area variation series cavitated on the pressure-side.
7. A Wageningen B-series propeller (P 538) had more suction-side cavitation in the top position than the corresponding propeller in the propeller series tested (P 754). On the other hand it was free from pressure-side cavitation.
8. Small systematic variations (mean line curvature and edge radius) at the leading parts of the profiles have been investigated. The influence on pressure-side cavitation in most cases was very marked, whilst the influence on suction-side cavitation was negligible.
9. The older propellers designed according to the principles in Table 2 (P 754—P 756) cavitated along the leading edge of the pressure side, when the blades were in their outer positions (90° and 270°). This type of cavitation was completely eliminated for propellers Nos. P 905—P 907, designed according to Table 3. The extent of suction-side cavitation was similar for the new propeller family and the corresponding older propeller, P 755.
10. The variation of the profile thickness distribution did not give any significant differences.
11. From the analysis of model cavitation tests and ship propeller erosion pictures, it can be concluded that the model tests give an indication of danger of propeller erosion.

## 8. Acknowledgements

This paper was published with the approval of Dr. HANS EDSTRAND, Director of the Swedish State Shipbuilding Experimental Tank, who also encouraged the work with advice and ideas. The author also would like to express his gratitude to Mr. B. HOLMER, who carried out most of the cavitation tests and Mr. E. BJÄRNE, who assisted with the analysis of the material and the preparation of the report.

## 9. References


[1] FREIMANIS E., LINDGREN H.: "Systematic Tests with Ship Models with $\delta pp = 0.675$, Part I", *Publ. No. 39 of the Swedish State Shipb. Exp. Tank (SSPA)*, Göteborg 1957.

[2] LINDGREN H., JOHNSSON C.-A.: "The Correlation of Ship Power and Revolutions with Model Test Results", *SSPA Publ. No. 46*, Göteborg 1960.

[3] *ITTC Propulsion Committee, Report to the Ninth International Towing Tank Conference*, Paris 1960.

[4] VAN MANEN J. D., LAP J. W.: "Scale Effect Experiments on Victory Ships and Models, Part II", *Trans. RINA, Vol. 100*, London 1958.

[5] VAN MANEN J. D.: "Propeller Experiments in Irregular Flow Distribution", *Appendix 6 of the Propeller Cavitation Committee Report, Ninth ITTC* Paris 1960.

[6] LEWIS F. M., TACHMINDJI A. J.: "Propeller Forces Exciting Hull Vibration", *Trans. SNAME, Vol. 62*, New York 1954.

[7] LERBS H.: "On the Effects of Scale and Roughness on Free Running Propellers", *Journal ASNE, Vol. 63*, No. 1, Washington 1951.

[8] LINDGREN H.: "The Cavitation Laboratory of the Swedish State Shipbuilding Experimental Tank", *SSPA Publ. No. 43*, Göteborg 1958.

[9] LINDGREN H., JOHNSSON C.-A.: "Propellerberäkning enligt virvelteorien. Räkneexempel och hjälpdiagram", *SSPA Allmän rapport No. 2*, Göteborg 1956.

[10] VAN MANEN J. D., VAN LAMMEREN W. P. A.: "The Design of Wake-Adapted Screws and Their Behaviour Behind the Ship", *Int. Shipb. Progress, Vol. 2, No. 7*, 1955.

[11] ECKHARDT M. K., MORGAN W. B.: "A Propeller Design Method", *Trans. SNAME, Vol. 63*, New York 1955.

[12] KRAMER K. N.: "Induzierte Wirkungsgrade von Best-Luftschrauben endlicher Blattzahl", *Luftfahrtforschung, Bd. 15*, Berlin 1938.

[13] LERBS H.: "Ergebnisse der angewandten Theorie des Schiffspropellers", *Jahrbuch der Schiffbautechnischen Gesellschaft, Bd. 49*, 1955.

[14] GINZEL J., LUDWIEG H.: "Zur Theorie der Breitblattschraube", *Aerodynamische Versuchsanstalt Göttingen, Bericht 44/A/08*, 1944.

[15] BURRILL L. C.: "Developments in Propeller Design and Manufacture for Merchant Ships", *Trans. IME*, 1943.

[16] VAN LAMMEREN W. P. A., TROOST L., KONING J. G.: "Resistance, Propulsion and Steering of Ships", 1948.

[17] SHULTZ J. W.: "The Ideal Efficiency of Optimum Propellers Having Finite Hubs and Finite Number of Blades", *DTMB Report 1148*, Washington 1957.

[18] TACHMINDJI A. J., MILAM A. B.: "The Calculation of the Circulation Distribution for Propellers with Finite Hub Having Three, Four, Five and Six Blades", *DTMB Report 1141*, Washington 1957.

[19] VAN MANEN J. D., CROWLEY J. D.: "Some Aspects of Circulation Theory Design of Screw Propellers", *Int. Shipb. Progress, Vol. 6*, 1959.

[20] PASCAULT J.: "Réflexions sur l'érosion de cavitation observée sur des hélices de cargos et de pétroliers à une seule ligne d'arbres", *Bulletin ATMA No. 60* Paris 1960.